SEISMIC VULNERABILITY ASSESSMENT OF MASONRY INFILLED RC FRAME STRUCTURES IN PAKISTAN

By

Hafiz Abdul Aleem

(2010 -NUST - MS PhD - Str - 07)

A thesis submitted in partial fulfillment of

the requirements for the Degree of

Master of Science

in

Structural Engineering

NUST Institute of Civil Engineering (NICE)

School of Civil and Environmental Engineering (SCEE)

National University of Sciences and Technology

Islamabad, Pakistan

(2013)

ABSTRACT

The influence of masonry infills on seismic response of reinforced concrete frame structures is one of the major fields of investigation for civil engineers in last few decades. Literature from proceedings of years of researches reveals that the effects of masonry infills are far from negligence; both for their beneficial effects (higher resistance to lateral loads, higher stiffness, improved energy dissipation capacity) and for their adverse ones (increase in seismic demand, possible mechanism of shear failure in frame members). Contrary to that, due to large number of parameters involved in modeling of infill panels, diversities in construction practices in different parts of world and influence of workmanship, no convergence has been reached on the adoption of unique model in the analysis by the experts.

This study is aimed at the development of a frame work for the seismic vulnerability assessment of masonry infilled reinforced concrete frame structures taking Pakistan as a case study. In this research various techniques available in literature for analytical modeling of infill panels are studied, out of which three strut model is employed. As this research is focused on Pakistani buildings, therefore, testing is conducted to evaluate the compressive strength of typical Pakistani brick masonry required for material modeling of the equivalent struts.

A two dimensional single bay, two storey frame has been modeled in Finite element software with three equivalent struts in each direction. After the modeling, non-linear static cyclic analysis is carried out and the hysteresis loop obtained is compared with the other experimentally obtained hysteresis loops investigated by the other researchers. Based on the capacity curve obtained from hysteresis loop, vulnerability curve for masonry infilled RC frame structure is derived using the procedure proposed by Kyriakides (2007) and is compared with that of bare frame derived by Qayyum (2012) and GESI expert opinion based curve.

ACKNOWLEDGEMENTS

Indeed, all praise and glory is for Allah, who is the Lord of the worlds and all my success is due to His blessings.

I am extremely grateful to my supervisor Dr. Shaukat Ali Khan for his extensive support, encouragement and guidance throughout my dissertation preparation.

I owe gratitude to my friends Kashif Qayyum, Hammad Salahuddin and Muhammad Arslan for their help and guidance during this thesis work.

My heartiest words of gratitude for my father and mother whose prayers and love has always made me succeed in life. Whatever I have achieved is because of their efforts and prayers.

This dissertation is dedicated to my parents and siblings.

Table of Contents

LIST OF FIGURES

LIST OF TABLES

Chapter 1

1 INTRODUCTION

1.1 Introductory Remarks

The construction of multi-storey buildings is associated with infilled frames. In most of the constructions especially in developing countries such as Pakistan, masonry is used for infills because it is faster, easier and even cheaper than other materials used for their construction. The materials commonly used for masonry infill walls are burnt clay bricks, hollow concrete blocks and hollow clay tiles.

The infills surrounded by reinforced concrete frames provide enclosure and internal partitioning to the buildings. As their use is aesthetic or functional rather than structural, therefore, they are considered as non-structural elements and their presence is neglected in design process. However, in past earthquakes, the performance of such buildings has revealed that presence of masonry infills alter the global response of buildings significantly under lateral loading (Degefa, 2005). During the earthquakes masonry infill walls interact extensively with the surrounding RC frames and change the stiffness of structures (Rodrigues et.al, 2008).

A misconception is present amongst some researchers that the presence of infill in RC frame always improves the lateral load capacity. However, past earthquakes proved that the statement is usually incorrect (WHE, 2006). Earthquake damage has been observed by the structural modification of frame caused by infill panels as shown in figure 1.1, where fracture of columns can be observed in the vicinity of column-beam joints. Masonry walls increase the stiffness of RC frame building and change its intended structural response by acting as diagonal struts. The shear stresses developed by this phenomenon are transmitted to the columns and generate high shear forces in them, thus, making them more vulnerable to shear failure (Degefa, 2005).

Figure 1.1: Failure of masonry infill walls due to the diagonal compressive forces transferred from column-beam joint, during Kashmir (2005) earthquake (Javed, 2009).

(a) **(b)**

Figure 1.2: Failure along diagonals in masonry infill panels. (a) R. Vicente, 2010 (b) kappos, 2009.

The catastrophic events caused by past earthquakes lead to requirement for the development of evaluation plan generally known as Earthquake risk assessment (ERA) to depict the expected structural response of structures during seismic excitations. For the mitigation of earthquake risks, ERA is a first step for which vulnerability assessment and seismic hazards are required. The purpose of these is to develop damage indicators of structures for various levels of hazards and show them with vulnerability curves (Kyriakides, 2007).

The vulnerability of buildings varies in different places of world due to the diversities in construction practices and available materials. The work done on masonry infilled RC frame structures in Pakistan is not significant.

1.2 Aims and Objectives

Aims

The aim of this study is to develop a frame work for the seismic vulnerability assessment of masonry infilled reinforced concrete frame structures taking Pakistan as a case study.

Objectives

- Review of literature for the behavior of RC frame structures with masonry infill panels along with their modeling techniques.
- Experimentally determine the strength of typical Pakistani masonry.
- Analytical modeling and analysis of masonry infilled RC frame structure.
- Development of seismic vulnerability curve for masonry infilled RC frame structures using the procedure proposed by Kyriakides (2007).
- Comparison of masonry infilled and bare frame vulnerability curves.

1.3 Dissertation Structure

Chapter 2 is based on the literature review. In this chapter a discussion on the masonry infills is presented along with the general response of RC frames containing these infills. Different failure modes and the various modeling techniques available in literature for these infills are also discussed in this chapter. In the end a brief discussion on seismic vulnerability assessment is presented.

Chapter 3 presents the experimental testing carried out to determine the compressive strength of typical Pakistani brick masonry required for material modeling of equivalent struts. For the preparation of samples, cement-sand mortar and locally manufactured bricks collected from different sources were used.

Chapter 4 discusses detailed structural modeling of infilled RC frame along with the appropriate models selected to form analytical building model. The modeling techniques and methodology adopted are also discussed in this chapter.

Chapter 5 includes the nonlinear static cyclic analysis carried out on RC frame modeled with three equivalent struts. Then the results obtained from the analysis in terms of hysteresis loop are discussed. Finally, these results are used to derive the vulnerability curve for masonry infilled RC frame structure.

Chapter 6 is the final chapter presenting the conclusions drawn as a result of this study and providing the recommendations for future work.

Chapter 2

2 LITERATURE REVIEW

2.1 Introduction

This chapter presents masonry infills along with their general response in reinforced concrete frame structures. Different failure modes of infill panels are discussed in this chapter and then various techniques used during last few decades for the analytical modeling of infills are reviewed. After that few analytical models for the shear strength of Reinforced concrete frame members are provided in order to capture the behavior of masonry infilled RC frames.

Finally a discussion on seismic vulnerability assessment is presented. Different aspects and methods for vulnerability assessments are discussed along with their merits and demerits. Various methodologies and their effectiveness for reinforced concrete structures are discussed. The extensively used analytical vulnerability assessment method is emphasized. Several related aspects such as selection of analytical tool, capacity models, damage indices and for the determination of parameters of response, methods of analysis are also discussed.

2.2 Masonry Infilled RC Frames

Unreinforced masonry infill walls confined by reinforced concrete frames have been constructed worldwide for more than 200 years. They fill in the portal spaces inside bounding frames. In such type of composite structural system, frames carry gravity loads while non-load bearing infill panels provide internal partitioning and enclosure to the buildings. Masonry infills are considered as nonstructural elements and are not considered in design process. However, these infills interact with the bounding frame and alter the actual behavior of the building substantially especially under seismic loading.

In Pakistan most of the buildings, from small houses to multistory commercial and residential complexes, contain unreinforced masonry as infills. These infill panels are in full

contact with the surrounding frames, as shown in Fig 2.1. However, in the commercial design practice in Pakistan, the effect of these infills is not taken into account making their seismic response unpredictable.

Masonry infills have been experimentally investigated since 1950s and experimental results, as well as field performance, indicate that infills change strength, stiffness and energy dissipation characteristics of the system when compared to the bare frame (Tucker, 2012).

Based on the analytical study of the seismic performance of masonry infilled RC framed structures, Kappos (2000) found that analysis results in increased stiffness by as much as 440%, when masonry infills are taken into account. Based on the design earthquake spectral characteristics, the dynamic behavior of infilled frame can be significantly different from that of bare frame. Kappos also presented that more than 95% of the energy is dissipated in masonry infills by their cracking at serviceability level. While at higher levels, RC frame starts making a considerable contribution. This clearly verifies that initially masonry infills resist the forces induced by earthquake loading whereas RC frame is critical for the performance of the structure at stronger excitations especially beyond the design earthquake (Asteris et al, 2011).

Masonry infill panels consists of variety of materials like clay bricks, concrete masonry units or concrete hollow blocks and hollow clay tiles etc. however, this research will be restricted to clay bricks only.

Figure 2.1: Brick masonry infill with concrete frame.

2.2.1 General Response of Masonry Infill System

Several stages of in-plane loading response occur with a masonry infill system. Initially, the system acts as a monolithic cantilever wall whereby slight stress concentrations occur at the four corners, while the middle of the panel develops an approximately pure shear stress state. As loading continues, separation occurs at the interface of the masonry and the frame members at the off-diagonal corners. Once a gap is formed, the stresses at the tensile corners are relieved while those near the compressive corners are increased (Tucker, 2012).

As the loading continues, further separation between the masonry panel and the frame occurs, resulting in contact only near the loaded corners of the frame. This results in the composite system behaving as a braced frame, which leads to the concept of replacing the masonry infill with an equivalent diagonal strut as shown in Figure 2.2.

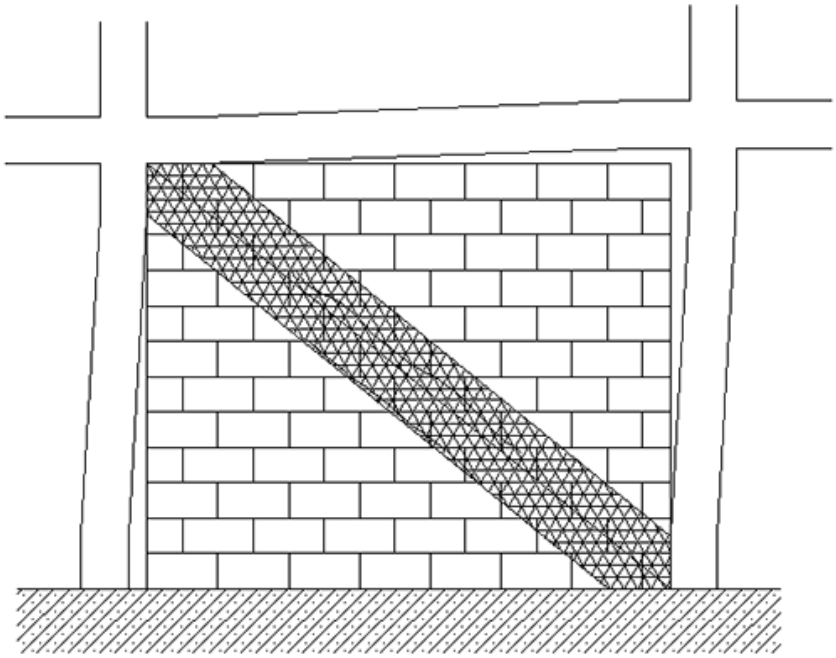

Figure 2.2: Diagonal strut concept (Tucker, 2012)

2.2.2 Failure Modes of Infilled RC Frames

The failure mechanisms affecting the components of the infilled frames are referred to as failure modes. The final failure of the structure is caused by either one principle mode or by the combination of different modes. Different failure modes for solid infill panel components were proposed on the basis of both analytical and experimental results obtained during last five decades (Thomas 1953; Wood 1958; Mainstone 1962; Liauw and Kwan 1983b; Mehrabi and Shing 1997), which can be classified into five distinct modes (Wood 1978; El-Dakhakhni 2002; Ghosh and Amde 2002; El-Dakhakhni et al. 2003). These are discussed below:

2.2.2.1 Bed-Joint Sliding

In this type of behavior mode sliding-shear failure of masonry panel occurs due to horizontal crack formation at about mid height of panel as shown in Fig.2.3. This phenomenon is usually accompanied by other failure modes. This failure mode was reported by Fiorato et al. [1970], Brokken and Bertero [1981, 1983] in tests of infilled reinforced concrete frames. This kind of failure is normally caused by weak mortar joints in brick masonry and large panel length as compared to its height.

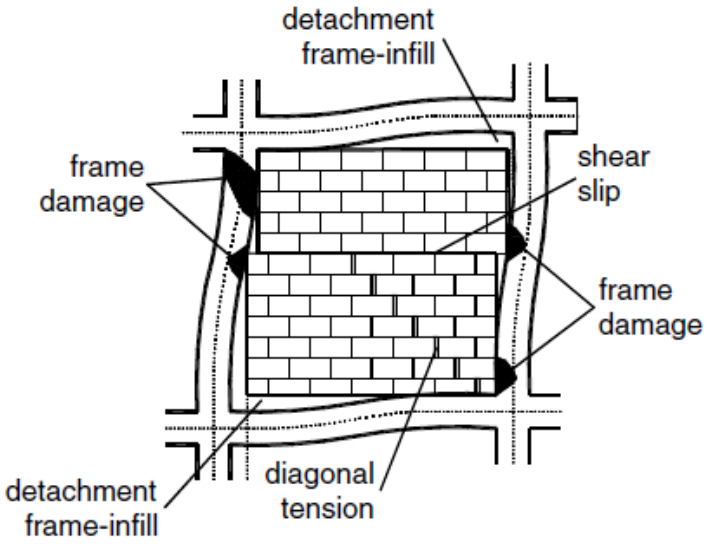

Fig 2.3: sliding shear mode; Diagonal cracking mode; Frame failure mode (Asteris et al, 2011)

2.2.2.2 Diagonal cracking

Diagonal cracking mode takes place across the compressed diagonal of the infill panel and most of the time occurs simultaneously with the sliding shear mode, as shown in Fig. 2.3. This behavior mode occurs when masonry units are weak in comparison with mortar joints or when either frame is weak or frame joints are weak with strong members and are infilled with strong panel (Mehrabi and Shing 1997; El-Dakhakhni 2002).

2.2.2.3 Frame Failure

In this type of failure mode support provided by infill panel cause plastic hinges to develop in columns at approximately mid height or in beam-column joints or may cause columns to fail in shear as shown in Fig. 2.3. This behavior mode occurs when either frame is weak or frame joints are weak with strong members and are infilled with rather strong panel (Paulay and Pristley, 1992).

2.2.2.4 Corner Crushing

Corner crushing occurs due to high stresses in each corner of diagonal compression under lateral loading of infill panel, as shown in Fig. 2.4. This behavior mode occurs when infill panel is weak and the surrounding frame has strong members and weak joints (Mehrabi and Shing 1997; El-Dakhakhni 2002; Ghosh and Amde 2002; El-Dakhakhni et al. 2003).

2.2.2.5 Diagonal Compression

In Diagonal compression infill panel crushes within its central region, as shown in Fig. 2.4. This mode occurs in relatively slender panel, in which failure is caused by out of plane buckling of infill.

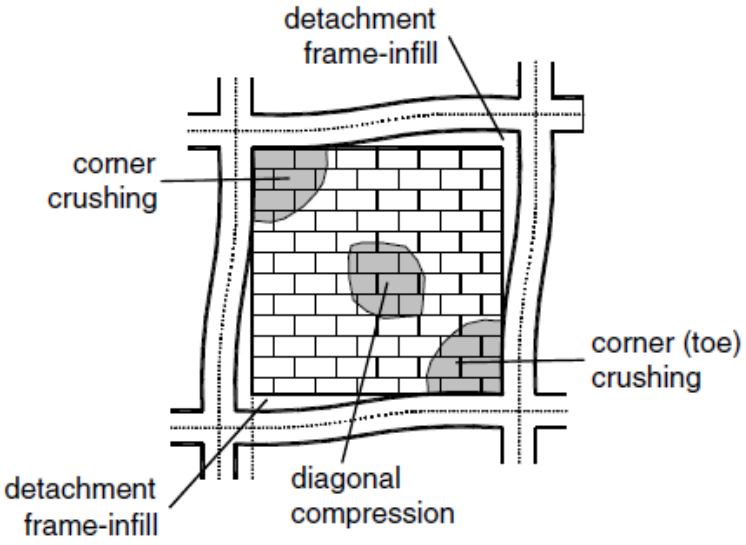

Figure 2.4: Corner crushing mode; Diagonal compression mode (Asteris et al, 2011)

2.2.2.6 Out of Plane Failure

This behavior is normally caused by the shaking of ground transverse to the plane of infill panel. This type of failure is more likely to take place in upper stories of high rise buildings where the floor accelerations are basically resonance amplifications of prominent sinusoidal ground motion input (FEMA 356).

2.2.3 Modeling of Masonry Infill Panels

Masonry infilled frames exhibit complex structural behavior integrating numerous factors. Experimental studies show that even at low-level loading, such type of structures show highly nonlinear inelastic behavior. Material nonlinearity initiates from the material properties i.e. degradation of both the surrounding frame and the infill panels, variation of contact length, and the loss of bond friction mechanism at the interface, etc. geometric nonlinearity also affects the behavior of infilled frame considerably, especially when structure is resisting large lateral displacements. The above mentioned nonlinear effects cause analytical complexities

which require sophisticated computational techniques for their proper consideration in the modeling.

Due to strength and stiffness degradations occurring in cyclic loading, the masonry infilled frames cannot be modeled as elasto plastic systems, rather more realistic models are required to obtain valid results (Zhang, 2006).

The several analytical techniques have been proposed in the literature in order to idealize this structural type. These models can be classified into two groups, namely, local or micro models and simplified or macro models. In first group, to take into account the local effects in detail, the structure is divided into various elements while in second group simplified models are used which are based on the physical understanding of the general behavior of the infill panels and to represent the effects of masonry panels very few elements are used.

2.2.3.1 Micro Models

Finite element method is used to represent the micro models. Malick and Severn (1967) First time used this approach to model infilled frame structures. In micro modeling different elements are used to model this approach such as beam elements are used for frame modeling, plane frame elements for modeling infill panels and interface elements for interaction between panel and frame.

Although this approach exhibits advantage in order to study the possible modes of failure in detail such as cracking, crushing and still its use is limited because of greater computational effort required and it also implies more time for modeling and analysis. After Malick and Severn (1967) other researchers worked on micro models are Gooman (1968), Riddington and Stafford Smith (1977), KIng and Pandey (1978), Rivero and Walker (1984), Liauw and Kwan (1984), Dhanasekar (1985), Chrysostomou (1991), Shing (1992), Syrmkezis and Asteris (2001) as suggested by Smyrou (2006).

2.2.3.2 Macro Models

In order to avoid the complexities and computational efforts associated with micro models researchers attempted to simplify the modeling of masonry panels in framed structures. Conceptual and experimental observations have indicated that a diagonal strut of suitable mechanical and geometrical characteristics could possibly provide a solution to the problem (Asteris et al, 2011).

2.2.3.2.1 Diagonal-Strut Models

Polyakov (1960), suggested that the effect of infill panel can be taken into account by replacing it with a single diagonal bracing. Subsequently Holmes (1961) adopted this suggestion and replaced the infilling with an equivalent pin jointed diagonal strut having same material and thickness as that of infill and width was taken equal to one third of strut length i.e.

$$\frac{w}{d} = \frac{1}{3} \qquad \text{Equation 2-1}$$

Where d =diagonal length of masonry panel. The one third rule was suggested as applicable regardless of relative stiffness of the infill and frame. Based on the experimental data of a series of experiments on steel frames, smith (1962) found that the w/d ratio varies from 0.1 to 0.25. (Smith 1966; Smith and Carter 1969), after additional experiments, proposed an analytical equation for width of diagonal strut by relating it to the contact length between infill and frame.

$$Z = \frac{\pi}{2\lambda} \qquad \text{Equation 2-2}$$

$$\lambda_h = h.\sqrt[4]{\frac{E_m t_w \sin(2\theta)}{4E_c I_p h_w}} \qquad \text{Equation 2-3}$$

Where

h=column height between centerline of beam

E_m = elastic modulus of masonry

t_w = Thickness of masonry panels

E_c = elastic modulus of frame

I_p= moment of inertia of column

h_w = height of masonry

θ = angle between infill height and bay length

$$\theta = tan^{-1}\left(\frac{h_w}{L_w}\right) \qquad \text{Equation 2-4}$$

L_w = length of infill panel

Mainstone (1971), suggested an empirical equation on the basis of analytical and experimental data, to calculate the equivalent strut width.

$$\frac{w}{d} = 0.16\lambda_h{}^{-0.3} \qquad \text{Equation 2-5}$$

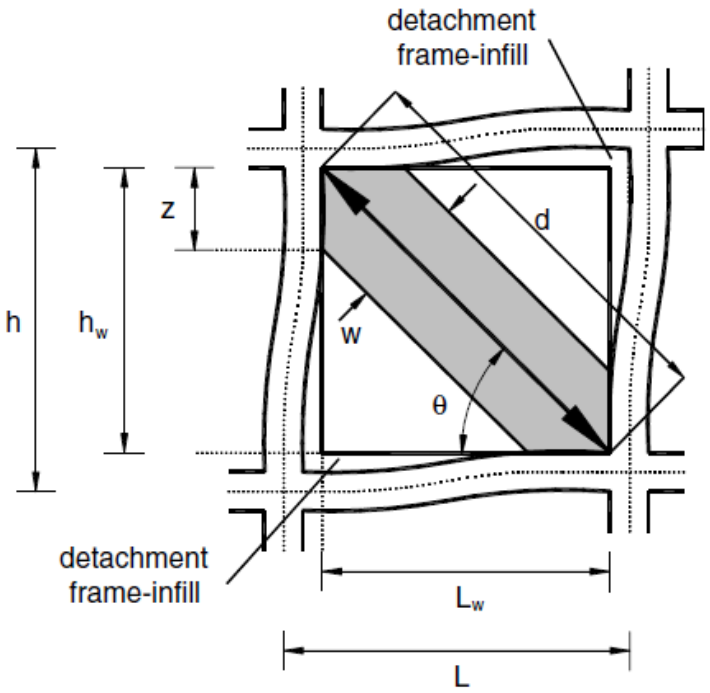

Figure 2.5: Masonry-infill frame sub assemblages (Asteris et al, 2011)

Weeks and Mainstone (1970) and Mainstone (1974), also suggested an empirical equation on the basis of analytical and experimental data, to calculate the equivalent strut width.

$$\frac{w}{d} = 0.175\lambda_h{}^{-0.4} \qquad \text{Equation 2-6}$$

The above formula was used in FEMA 274 (FEMA 1997) and FEMA 306 (FEMA 1998) because it was accepted by most of the researchers working on analysis of infilled frames (Klingner and Bertero 1978; Sobaih and Abdin 1988; Fardis and Calvi 1994; Negro and Colombo 1997; Fardis and Panagiotakos 1997; Kodur et al. 1995, 1998; Balendra and Huang 2003).

Liauw and Kwan (1984) suggested the following expression using the previous experimental data.

$$\frac{w}{d} = \frac{0.95sin2\theta}{2\sqrt{\lambda_h}} \qquad \text{Equation 2-7}$$

For practical engineering purposes, the values of angle θ in above equation were adopted equal to 25° and 50°.

Decanini and Fantin (1987), based on the on the results obtained from the masonry frame tested under lateral loading suggested two sets of equation considering cracked and uncracked masonry(Asteris et al, 2011). The variation of the ratio b_w/d_w as a function of parameter λ_h is shown in Figure 2.7.

$$\text{Uncracked panel: } \frac{w}{d} = \begin{cases} 0.085 + \frac{0.748}{\lambda_h} \; if \; \lambda_h \leq 7.85 \\ 0.130 + \frac{0.393}{\lambda_h} \; if \; \lambda_h > 7.85 \end{cases}$$

$$\text{Cracked panel: } \frac{w}{d} = \begin{cases} 0.010 + \frac{0.707}{\lambda_h} \; if \; \lambda_h \leq 7.85 \\ 0.040 + \frac{0.470}{\lambda_h} \; if \; \lambda_h > 7.85 \end{cases}$$

Paulay and Pristley (1992), considered a conservatively high value of diagonal strut width as it will result in a stiffer structure, and hence a potentially higher seismic response.

$$\frac{w}{d} = \frac{1}{4}$$ Equation 2-8

The variation of the ratio b_w /d_w for infill frames as a function of parameter λ_h as suggested by different researchers is shown in Figure 2.6.

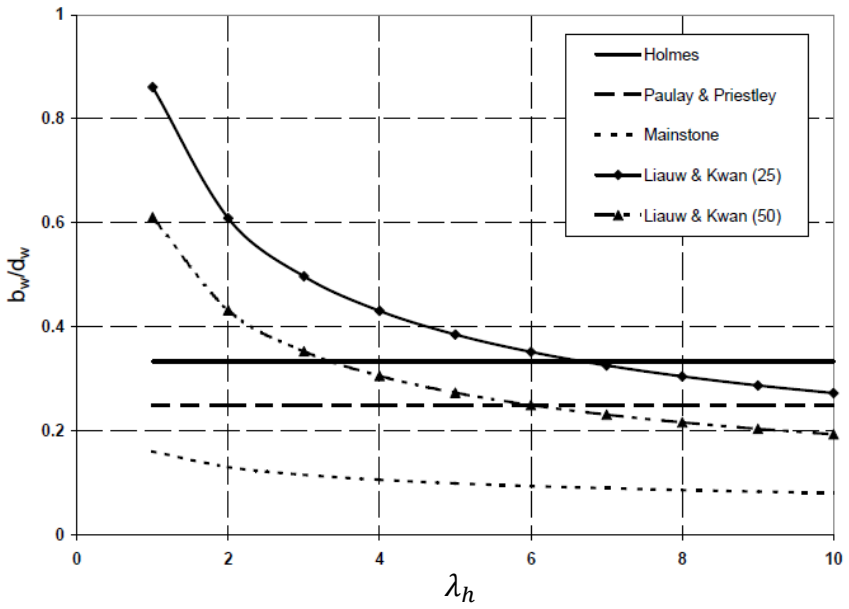

Figure 2.6: Variation of the ratio b_w /d_w for infill frames as a function of parameter λ_h (Ali, 2009)

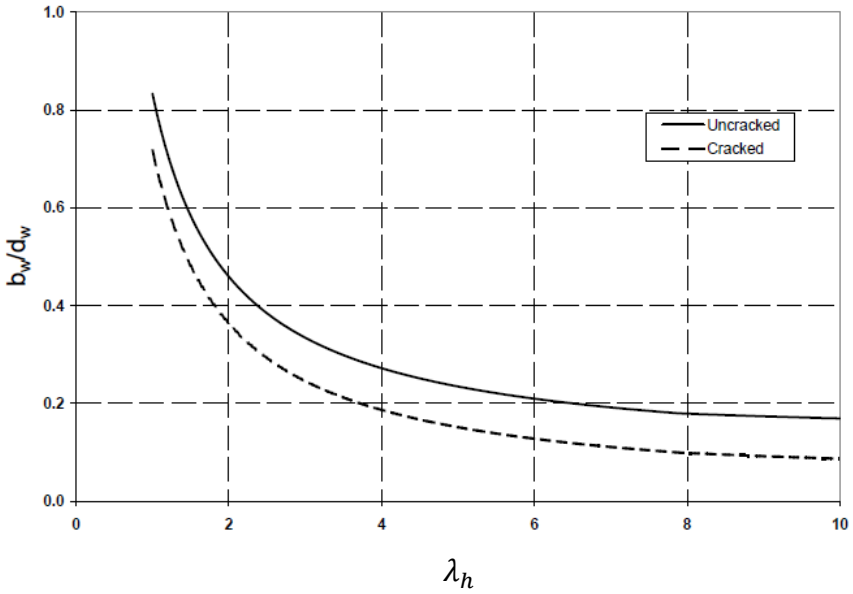

Fig 2.7: Variation of the ratio b_w/d_w as a function of parameter λ_h (Decanini and Fantin, 1987)

2.2.3.2.2 Multiple-Strut Models

During the last two decades, it has become clear that the complex behavior of infilled masonry cannot be modeled using single diagonal strut. Many researchers (Reflak and Fajfar 1991; Saneinejad and Hobbs 1995; Buonopane and White 1999), reported that a single equivalent strut connecting two corners of the panel cannot adequately represent the shearing forces and bending moments in frame members. More complex macro-models comprising of more than one diagonal struts were proposed.

Despite the increased computational effort involved in multiple struts modelling, it is advantageous in a way that it represents the actions in frames more accurately. In frame members, to stress the significant effect of different contact lengths, Syrmakezis and Vratsanou (1986), employed in each diagonal direction, five parallel struts.

Chrysostomou et al. (1991) intended to obtain the performance of masonry infilled frame under lateral loading by considering both strength and stiffness degradation of infill panel. Chrysostomou proposed a model in which each infill panel contains six inclined struts having only compression as shown in Fig. 2.8.

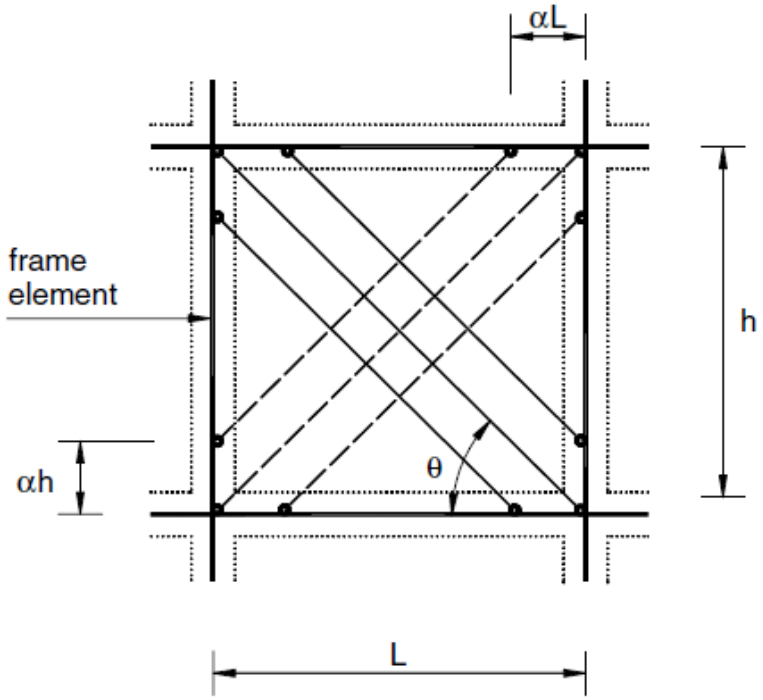

Figure 2.8: Six-strut model for masonry-infill panel in frame structures (Chrysostomou 1991).

In Chrysostomou (1991) six strut model, the off-diagonal struts are positioned at critical locations. These locations on the frame members are specified by a factor α, which is a fraction of height or length of a panel. This factor α, is associated with the plastic hinge formation in column or beam. Liauw and Kwan (1983a, b, 1984) gave the theoretical values for this factor. During the nonlinear analysis response, only three struts are active (in corresponding direction) at any point (Asteris et al, 2011).

Crisafulli (1997), studied the structural response of RC infilled frames using different multi-strut models, while focusing the stiffness of structure and induced actions in the surrounding frame. Numerical results, obtained from these different models were compared with refined finite element micro models. Lateral stiffness of infilled frame was similar in all cases with slightly smaller values for two and three strut models, however it was observed that stiffness of multi strut models alter significantly when separation between struts changes. It was also observed that the single strut model underestimates the shear forces and bending moments as lateral loads are mainly resisted by truss mechanism, whereas the double strut model leads to much larger values. On the other hand, a three strut model showed better approximation (Ali, 2009).

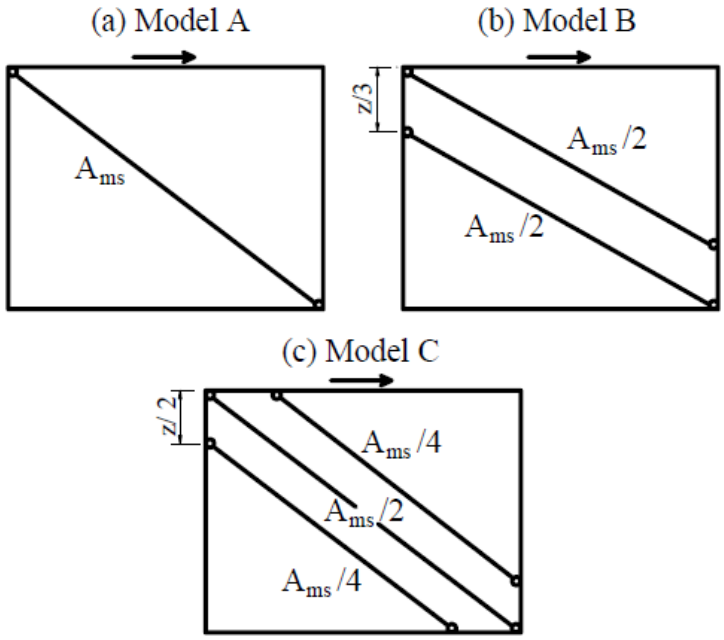

Figure 2.9: Modified strut models Crisafulli (1997)

Crisafulli and Carr (2007) suggested a new macro model in a simple but rational way. The model is applied as a four node panel element attached to the frame at column-beam joint. The panel element internally accounts for shear and compressive behavior separately using in each direction a shear spring between two parallel struts, as shown in Fig. 2.10. This configuration allows a satisfactory consideration of horizontal strength and stiffness of panel, especially when a diagonal tension failure or shear failure along mortar joints is expected. Although this model is easy to apply but it has a limitation that it is unable to predict the shear forces and bending moments in the surrounding frame adequately because it is connected to beam column joints of the frame.

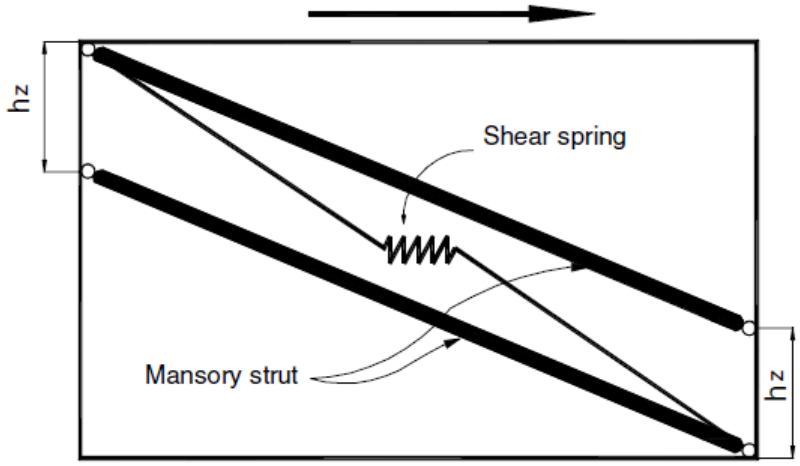

Figure 2.10: Proposed multi-strut model by Crisafulli and Carr (2007) for masonry-infill panel (only the struts and the shear spring active in one direction are represented)

2.2.3.3 Conclusion

From the above discussion it is evident that the single strut macro-models are not adequate to accurately represent the interaction between infill panel and the surrounding frame and hence they are unable to appropriately predict the force distribution in the members of the surrounding frame. Researchers attempted to represent the infill panels with multiple struts. Models have been proposed with two, three, and more than three struts. The merits and limitations of each of these models have been discussed and it is concluded that three strut models can represent infill frame interaction more accurately than the other models, but with increased complexity.

2.2.3.4 Strength of the Equivalent Struts

The shear and compressive strength of masonry infills depends on the properties of their constitutive materials, such as characteristics of bricks, compressive strength of mortar and hydration conditions at the brick-mortar interface. The superior quality of the constitutive materials yields stronger masonry, however it does not necessarily enhance the lateral strength of masonry infilled frame, as excessively strong masonry may result in premature failure of the frame members (Zhang, 2006).

To perform a nonlinear analysis of masonry infilled frame structure, a force-deformation relationship corresponding to equivalent strut model must be appropriately defined. The modeling of hysteretic behavior not only increases the computational complexity but also the uncertainties of the problem (Asteris et al, 2011).

The force displacement relationship of infill strut material is shown in Fig. 2.11. To determine the maximum strength of infill, Zarnic and Gostic (1997) proposed an equation validated by a set of experiments on single storey, single bay and two storeys, two bay infilled frames. Dolsek and Fajfar (2008) later modified this equation (Sattar and liel, 2010).

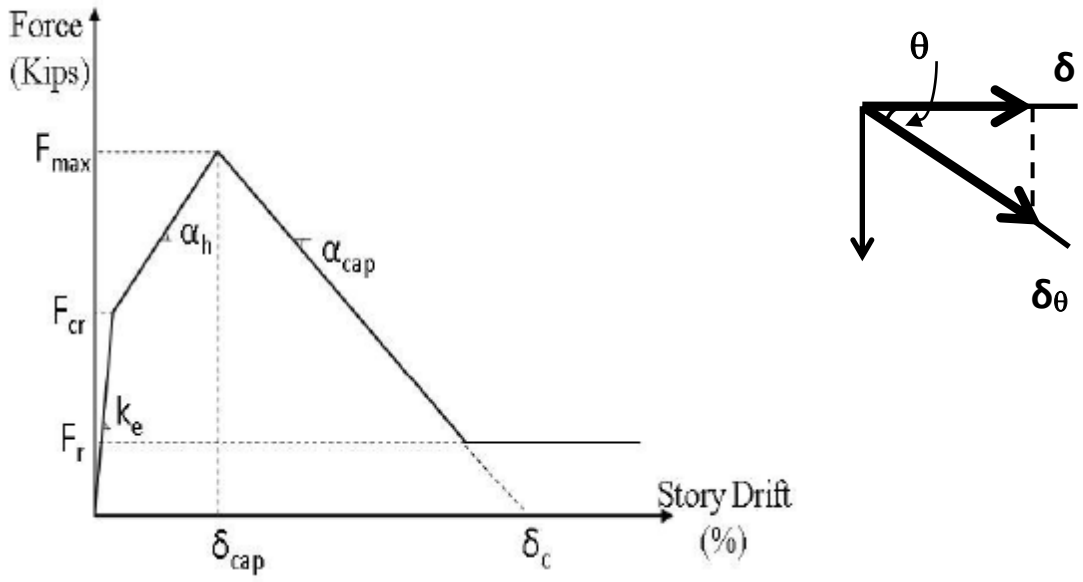

Figure 2.11: Force displacement behavior for infill strut material (Sattar and liel, 2010).

$$F_{\max} = 0.818\frac{L_{in}\, t\, f_{tp}}{C_I}(1+\sqrt{C_I^{\,2}+1}), \qquad C_I = 1.925\frac{L_{in}}{h'}$$

Equation 2-9

$\delta_\theta = \delta/\cos\theta$

The initial stiffness of masonry infill is

$$k_e = 2(E_m wt / L)(\cos\theta)^2$$

Equation 2-10

Where

L_{in} = Length of the infill.

f_{tp} = Cracking stress of the masonry.

t = Thickness of the infill.

h' = Height of the infill.

L = Length of the diagonal strut.

The deformation capacity of the masonry infill panel is based on the observations from experimental tests and recommendations provided by past researchers. Experimental results (Manzouri, 1995) showed that the displacement against maximum force (i.e. δ_{cap} in Fig. 2.11) occurs at approximately 0.25% drift. Similarly, a series of experiments performed by Shing et al. (2009) found that in the frame specimen, the maximum load occurs at about 0.25% drift. Dolsek and Fajfar (2008) estimated that the displacement against zero wall strength (i.e. δ_c in Fig. 2.11) is around five times the displacement at maximum force (δ_{cap}). A series of experiments reported in Carvalho and Coelho, Eds. (2001) supported the characteristics parameters of infills proposed by Dolsek and Fajfar (2008). Based on the experimental data, as reported in (FEMA, 1998), the residual strength (Fr) of masonry infill panel after its failure, vary from approximately 30% to 60% of the maximum strength (Sattar and Liel, 2010). Lawrence and Morgan suggested the value of cracking stress for masonry as 30 % of its ultimate strength plus 29 psi (Harry A. Harris, 1988). The shear strength of masonry is experimentally calculated as 6% of the compressive strength by Naseer (2009).

2.3 Shear Strength of RC Frame Members

As discussed earlier in section 2.2.2 that the masonry infills change the forces in the frame members, especially when masonry panel is strong, it increases the shear forces in columns particularly in top and bottom portions and column will be more vulnerable to fail in shear rather than in compression.

In this research the six strut technique will be used for infill modeling as it is discussed in section 2.2.3.3 that it gives better approximation. To study the effect of off-diagonal struts on the shear forces of frame members, shear force-displacement relationships are to be adequately defined.

2.3.1 Models for Shear Strength

For the evaluation and design of reinforced concrete members for shear, several models have been suggested and used during last few decades. These models show differences in terms of parameters and the approaches used to develop the equations. According to most of these models, shear strength is computed as summation of contribution of strength from concrete and transverse reinforcement. However, the effects of different parameters such as displacement ductility, axial load and aspect ratio are either represented differently or not included (Sezen, 2002).

In the various shear strength prediction methods the shear capacities of frame sections presented are associated with their displacement ductility, which is the ratio of the total imposed displacements Δ at any instant to that at the onset of yield Δ_y (Paulay and Priestley, 1992).

$$\mu = \Delta / \Delta_y > 1 \qquad \text{Equation 2-11}$$

Few of these models are discussed below:

2.3.1.1 ACI 318-11 (2011)

The equations provided in ACI 2011 for shear strength are deign equations, however, shear strength of existing RC members can be estimated using these equations. The shear strength capacity is calculated as sum of contribution of strength from concrete and transverse reinforcement.

$$V_n = V_c + V_s \quad \text{Equation 2-12}$$

For members subject to shear and flexure only, the contribution of shear strength from concrete is

$$V_c = 2\sqrt{f'_c}\, b_w d \quad \text{Equation 2-13}$$

For members subjected to shear and axial compression

$$V_c = 2\left(1+\frac{P}{2000\,A_g}\right)\sqrt{f'_c}\, b\, d \quad \text{Equation 2-14}$$

Where f'_c is the specified compressive concrete strength, P is the axial load, A_g is the gross cross-sectional area, and d and b are the effective depth and web width of the section, respectively.

The contribution of transverse reinforcement is calculated as

$$V_s = \frac{A_{sw} f_{yw} d}{s} \quad \text{Equation 2-15}$$

Where f_{yw} is the yield strength of transverse reinforcement and A_{sw} is the transverse reinforcement area within spacing, *S*, in the loading direction.

2.3.1.2 ASCE-ACI Committee 426 Proposals (1973, 1977)

In 1973, a report was published on shear strength of Reinforced concrete members by ASCE-ACI Joint Committee 426. This report was written in response to the damages observed in the 1971 San Fernando earthquake. In 1977, its revised version was published. Reasons for unwanted shear failure of RC members were investigated in 1973 report (Sezen, 2002).

According to this report, members subjected to axial compression, the contribution of concrete was calculated by

$$V_c = v_c \left(1 + \frac{3P}{f'_c A_g}\right) b\, d$$

Equation 2-16

For normal weight concrete members in which axial tension exceeds

$$0.5\sqrt{f'_c}\, A_g$$

Equation 2-17

Shear strength of concrete was calculated by

$$V_c = v_c \left(1 + \frac{P}{6\sqrt{f'_c}\, A_g}\right) b\, d$$

Equation 2-18

Where v_c is the shear stress carried by concrete and is calculated as

$$v_c = (0.8 + 100\,\rho_l)\ \sqrt{f'_c} \le 2.0\ \sqrt{f'_c}$$

Equation 2-19

Where ρ_l is the longitudinal reinforcement ratio ($\rho_l = A_s / (bd)$). The contribution of transverse reinforcement is same as given in ACI 318-11.

2.3.1.3 Aschheim and Moehle (1992)

Laboratory data from column tests of cantilever bridge was used by Aschheim and Moehle (1992), which indicated that the shear strength of column is a function of axial load, the quantity of transverse reinforcement and displacement ductility demand μ_δ. The shear strength capacity is calculated as sum of contribution of strength from concrete and transverse reinforcement. The contribution of transverse reinforcement is same as given in ACI 318-11 and contribution of concrete V_c is

$$V_c = \alpha'\left(1 + \frac{P}{2000\,A_g}\right)\sqrt{f'_c}\ b\,d \le 3.5\sqrt{f'_c}\,b\,d$$

Equation 2-20

For evaluation and design of reinforced concrete columns with rectangular hoops

$$\alpha' = \frac{0.0060\,\rho_w f_{yw}}{\mu_\delta}$$

Equation 2-21

Where ρ_w is the transverse reinforcement ratio, $\rho_w = A_{sw}/(bs)$.

2.3.1.4 Priestley et al. (1994)

Priestley et al. (1994), proposed that under cyclic lateral loads, the shear strength of columns can be calculated by summation of contribution from truss mechanism or transverse reinforcement, V_s arch mechanism related to axial load, V_p and concrete strength, V_c.

$$V_n = V_{c+} V_{s+} V_p$$ Equation 2-22

Concrete contribution is given by

$$V_c = k\sqrt{f_c'}\,A_e$$

Equation 2-23

Where A_e is equal to $0.8A_g$ and parameter, *K,* depends on the displacement docility of member as defined in Fig. 2.12. It is shown in Fig. 2.12 that with increasing displacement ductility, the contribution from concrete reduces to as much as 66 percent.

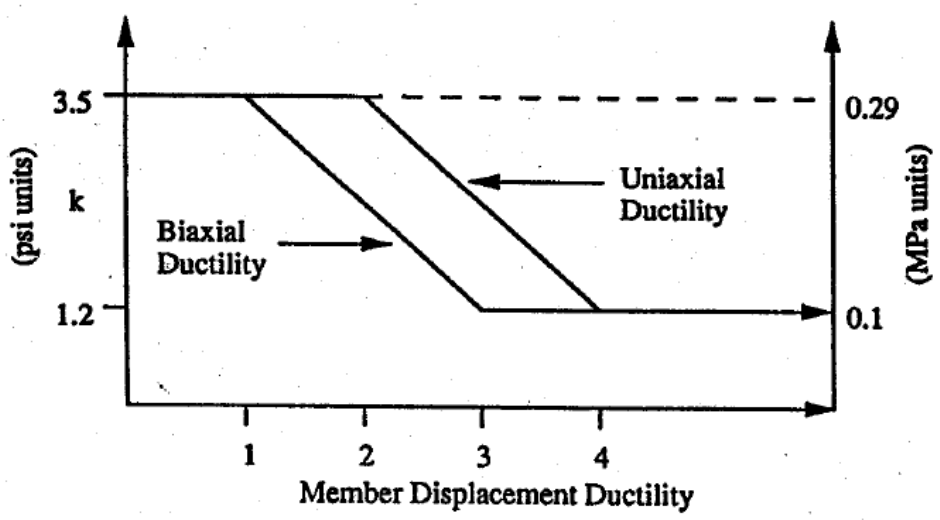

Figure 2.12: Concrete shear strength degradation with displacement ductility (Priestley et al. 1994)

The contribution to shear strength from transverse reinforcement is truss mechanism and uses 30^o angle between the column longitudinal axis and diagonal compression struts, for rectangular sections.

$$V_s = \frac{A_{sw} f_{yw} D'}{s}\cot 30^o$$

Equation 2-24

Where *D'* is the distance measured parallel to the applied shear between centers of the peripheral hoop.

The contribution from arch mechanism is given by

$$V_p = P \tan\alpha = \frac{D\text{-}c}{2a} P$$

Equation 2-25

Where α is the angle of diagonal compression, *c* is the neutral axis depth, and D is the overall depth of the section.

2.3.1.5 Sezen (2002)

Sezen (2002) proposed a shear strength model for columns based on the experimental tests which indicated that the shear strength of columns is influenced by various factors including aspect ratio, effective concrete area, concrete strength, amount of transverse reinforcement and axial load. According to this model total shear strength includes contribution from concrete and transverse reinforcement. The contribution from concrete is given by

$$V_c = \frac{6\sqrt{f_c'}}{a/d} \sqrt{1 + \frac{P}{6\sqrt{f_c'} A_g}} 0.80 A_g$$

Equation 2-26

For this equation the value of *a/d* is limited between 2 and 4. The contribution from transverse steel is calculated by

$$V_s = \frac{A_s f_{yw} d}{s}$$

Equation 2-27

Sezen (2002) proposed the force-deformation model for shear strength of columns relating shear capacity with displacement ductility.

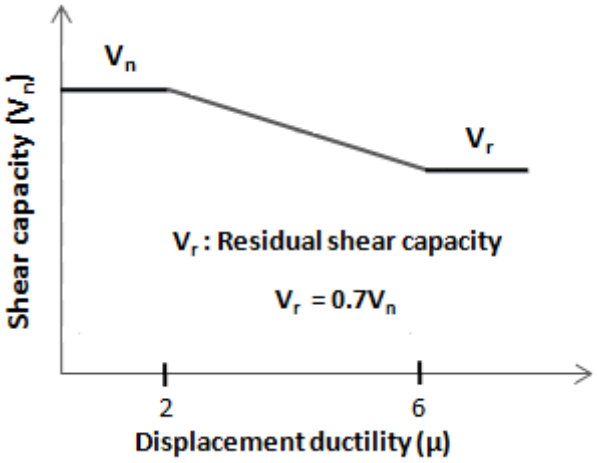

Figure 2.13: Shear strength model (Sezen, 2002)

Based on the shear displacement measured from experimental work, following equation was proposed by Sezen (2002) to calculate the value of shear displacement at yield.

$$\delta_{y,shear} = \left(\frac{3}{0.2 + 0.4P_r} \right) \frac{V_y L}{E_c A_g}$$

Equation 2-28

Where V_y = 2*My* /*L* for specimens with double curvature (M_y = moment capacity at yield), and P_r is axial load ratio, which is the ratio of the applied axial load, *P*, to the axial load capacity of the column, P_o.

$$P_o = 0.85 f_c' A_g (1 - \rho_l) + f_y A_{sl}$$

Equation 2-29

Discussion

The above discussed shear strength models are few of the available in the literature. Other models available are given by SEAOC (1973), Caltrans (1995), Architectural Institute of Japan, Structural Design Guidelines (1994), Kowalski et al. (1997), Konwinski (1996) and Konwinski et al. (1996), and FEMA-273 (1997).

In this framework shear strength model proposed by Sezen (2002) is more appropriate to be used as it provides equations with fewer parameters that are convenient to be modeled in the analytical tool (PERFORM 3D) used in this study.

2.4 Seismic Vulnerability Assessment

It has always been a great challenge for the earthquake engineering society to predict the damage potential from an earthquake. Whitman et al. (1974) attempted to quantify the expected potential of damage for different intensity levels, based on the 1971 San Fernando earthquake. The concept of Damage Ratio (DR) was first time developed by this study. DR is the ratio between repair and replacement value and at present it is the most widely used damage indicator for economy. Since then, several methods have been developed for vulnerability assessment differing in precision and level of detail.

The selection of the method depends mainly on the objective of assessment, availability of technology and type of data. For different levels of seismicity, these methods lead to damage quantification. Results obtained from different methods for same seismic exposure may differ from each other.

2.4.1 Methods for vulnerability assessment

There are four main approaches for earthquake vulnerability assessment (Ahmad, 2011).

- Empirical vulnerability assessment (based on observational data)
- Expert opinion (judgmental)
- Analytical vulnerability assessment (based on simplified or refined analysis)
- Hybrid vulnerability (combination of other types)

2.4.1.1 Empirical vulnerability assessment

Empirical methods are those which rely on historically obtained data for development of relationship between damage index and ground shaking intensity. Empirical vulnerability

assessment methods have been in practice since 1970's. The representation of hazard at that time was mostly based on the intensities such as Modified Mercalli Intensity (MMI) (Kyriakides, 2007).

Whitman (1974) was the first to relate Modified Mercalli Intensity (MMI) with damage in the form of Damage Probability Matrix (DPM), as shown in Table 2.1. The table shows DR=0 for no damage and DR=100 for collapse.

Table 2.1: Format of DPM after Whitman (1974)

Damage state	Structural damage	Non-structural damage	Damage ratio (%)	Intensity of Earthquake				
				V	VI	VII	VIII	IX
0	None	None	0-0.05	….	….	….	….	….
1	None	Minor	0.05-0.3	….	….	….	….	….
2	None	Localized	0.3-1.25	….	….	….	….	….
3	Not noticeable	Widespread	1.25-3.5	….	….	….	….	….
4	Minor	Substantial	3.5-4.5	….	….	….	….	….
5	Substantial	Extensive	7.5-20	….	….	….	….	….
6	Major	Nearly total	20-65	….	….	….	….	….
7	Building Condemned		100	….	….	….	….	….
8	Collapse		100	….	….	….	….	….

Rossetto (2002) related Spectral Displacement with PGA and developed vulnerability curves based on empirical data. Rossetto proposed six damage grades (from slight damage to collapse) and six types of design were developed for low, medium and high rise buildings and three types of codes (pre, old and new code) (Kyriakides, 2007).

2.4.1.2 Vulnerability Assessment by Expert Opinion

Expert Opinion or Expert Judgment is a very effective way of vulnerability assessment as unlike the empirical method unavailability of data is not an issue. But the outcomes of this method may be very subjective, as it is opinion based. First complete attempt on this method was by Applied Technology Council. It carried out expert judgment vulnerability assessment, on

buildings in California using MMI and Whitman's Damage Ratio (DR) as the parameters. 58 experts were hired for this job, with past experience in earthquakes from variety of areas.

The limitation of this method is that, to assign the weights and values of coefficients, it requires expert judgments, which in the behavior of building inherent uncertainties (Calvi and Pinho, 2006).

2.4.1.2.1 GESI Method

Geo-Hazards International (GHI) developed some basic vulnerability relations in their "Global Earthquake Safety Initiative pilot project" (GESI) (GESI, 2001). It included the expert's contribution from developing countries. For Pakistani conditions four basic building classes were defined. Their corresponding GESI curves (2001) are shown in Fig. 2.14.

a. RC framed structures (RCF)
b. RC framed structures with masonry infill. (RCI),
c. Unreinforced brick masonry (UBM),
d. Adobe and mud wall structures (adobe),

The contribution of experts from India, Indonesia, Japan, Ecuador, El Salvador, Mexico, Canada, Chile, Nepal, Pakistan, Philippines, Uzbekistan and Turkey was included in GESI project. To determine the suitable vulnerability curve, scoring scheme is used in GESI method, which includes the quality of materials, design and construction. The score is determined for the building type and the suitable vulnerability curve is allocated to a building class.

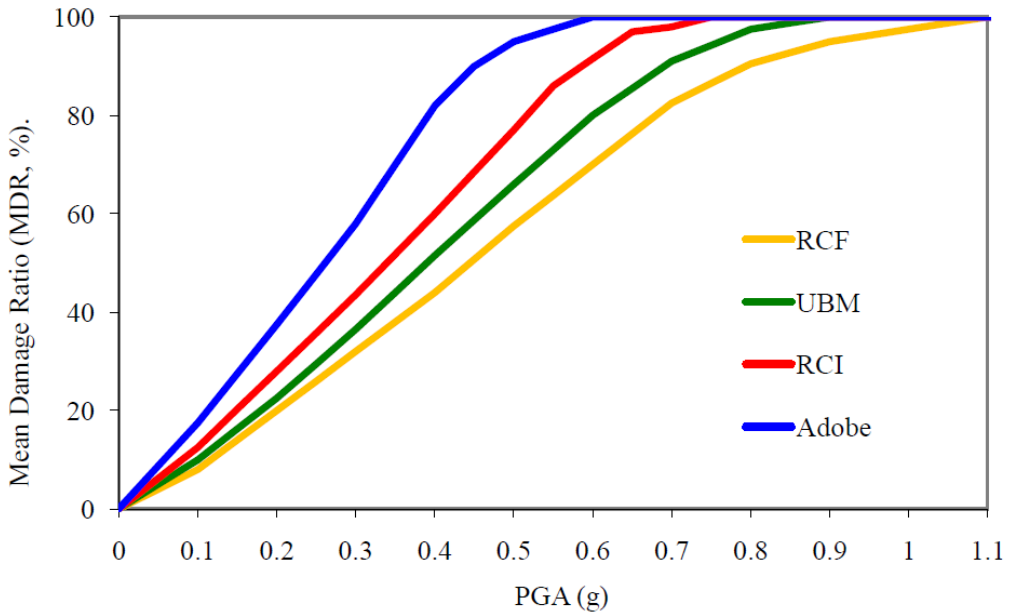

Figure 2.14: GESI (2001) vulnerability curves corresponding to the building classes found in the study area (for Pakistani conditions)

2.4.1.3 Hybrid Vulnerability

In hybrid vulnerability assessment other types of vulnerability assessment are combined i.e. empirical, judgmental and analytical. There are many uncertainties in the other techniques which are compensated in hybrid vulnerability assessment method. These uncertainties are attributed to limitations in post-earthquake data, issues related to modeling and subjectivity of judgmental data. To enhance the accuracy of output it is better to have data from various sources instead of one.

Many researchers worked in this field. Jalalian (2008) derived vulnerability curves for different buildings of Iran by combining the judgmental and empirical methodologies. Singhal and Kiremidjian (1996) used Bayesian approach by using Northridge earthquake damage data and derived vulnerability curves hence, updated the already available analytical vulnerability curves for mid-rise buildings (Kamran, 2011).

2.4.1.4 Analytical Vulnerability Assessment Method

The use of seismic vulnerability assessment has hiked in the recent past. Finite Element Analysis is performed by structure modeling using an analytical tool. Vulnerability curves were developed by Calvi (1999), Kyariakides (2007), and Ahmed (2011) by the use of above mentioned method.

After the hazard maps development in terms of spectral acceleration, contrary to seismic intensity level, more direct and more meaningful analytical methods were derived. They contain calibration of behavior, hazards and characteristics of structures. Regarding this feature, analytical vulnerability assessment methods are reflected to be of use for earthquake risk assessment, insurances and planning for decision making for disaster and risk mitigation. To cater for the demerits of empirical methods, computational analysis has been used in analytical vulnerability assessment in recent researches (Calvi and Pinho, 2006).

In this research, capacity spectrum method has been deployed for analytical vulnerability assessment. ATC-40 and FEMA 440 refer to the work of Kyriakides (2007) for the implementation of capacity spectrum method. For seismic vulnerability assessment, hazard and site spectrum response is selected. Then using this response spectrum, performance points and finally PGA is calculated. Response spectrum is a curve plotting maximum acceleration response of the corresponding single degree of freedom systems for numerous structures denoted by their time period on x-axis (SA vs. T). It is a jagged line for a specific earthquake, however for this study, design spectrum is used which is a smooth curve depend on site and soil state of affairs and is taken from UBC-97. Procedure for capacity spectrum will be elaborated in detail in chapter 5.

2.4.1.4.1 Analytical Method Used by Other Researchers

2.4.1.4.1.1 Kyriakides (2007)

Kyriakides initiated his research work through the vulnerability curves of Scanbel (1987) established for island of Cyprus. Kythreoti (2001) reasoned on these curves that they are extremely unpredictable because these were grounded on inadequate available data. Kyriakides got the data about PGA from Earthquake Rehabilitation service of Cyprus, then after examining the data he established PGA attenuation curves explicitly for Cyprus. These curves along with impaired data of numerous earthquake events were used by him to derive vulnerability curves for Masonry and RC structures. Those curves found are for the PGA ranging from 0.11g to 0.17g though only set of data existing was for 0.25g. Hence, analytical procedures were deployed to explore the characteristics of buildings at PGA >0.25g. Kyriakides went for analytical procedures by using a finite element software Drain 3D to notice the building's behavior.

DRAIN 3D was used comprehensively by many researchers but its precision for full scale tests and models was established by very few. Kyriakides tested DRAIN 3D capabilities of analysis by building a prototype of a two story Reinforced Concrete frame in the software and then calibrated this model by confirming the outcomes of this model at various intensities of PGA by the experimental results of full scale RC frame investigated in CEA research center in Saclay Paris, France. Analytical and experimental works are related by story displacements time histories at different levels of seismic exposure. The fallouts of DRAIN 3D were very near to experimental results, on this basis, Kyriakides established that DRAIN 3D is a tool that can be used dependably in analytical vulnerability assessment.

Response of structure was attained by static cyclic analysis in DRAIN 3D for medium and low rise frames using Eurocode-8 method of horizontal force distribution. Earthquake demand was denoted by response spectrum of Eurocode-8. Thus, by expending process of capacity spectrum Kyriakides derived the vulnerability curves and related those curves with vulnerability curves of Scanbel (1987). Lastly, he established that if there is accessibility of data then

empirical vulnerability curves are easily derived but its insufficiency is that it is not effective for unfamiliar buildings. Expert judgment methods are restricted due to the expert's opinion and reservations in the performance and enactment of the building. Therefore, when documentation of building damages in the past are not accessible then analytical methods are reliable and consistent.

2.4.1.4.1.2 Ahmed (2011)

Ahmed (2011) taking Pakistan as a case study did the seismic vulnerability assessment. He worked on mid and low rise Reinforced concrete structures with masonry infills. His research was the addition of the frame work suggested by Kyriakides (2007). He used the impaired data of Kashmir (2005) earthquake in his research work. He established the stress-strain models of low strength concrete and bond slip, after the experimental work. For vulnerability study, NSM was used and static cyclic analysis was carried out for the development of capacity envelope. Damage evaluation was completed by using damage index based on secant period normalized against collapse period.

2.4.2 Structural Damage Indicators

Damage Indicator is a physical value which correlates the structural response with damage potential in a structure. Cakmak and Di-Pasquale (1989) suggested a damaged index based on the development of the natural period of a time varying linear system corresponding to the actual non linear system. This damage index depends on the combined effect of stiffness degradation and plastic deformation (Ghobarah, 1999). In this global damage index the main drawback is that strength loss and dissipated hysteretic energy are not taken into account. Further, in this damage index maximum period calculation is also difficult (Kyriakides, 2007).

$$\boldsymbol{\delta_M = 1 - \frac{T_0}{T_{max}}} \qquad \text{Equation 2-30}$$

Where

T_0= Initial natural period,

T_{max}= Maximum natural period of the equivalent linear system

δ_M= Maximum Softening

For seismic evaluation Ghobarah (1999) developed an indicator and proposed a methodology in which two static nonlinear analyses are performed before and after subjecting the structure to an earthquake. Time-history analysis is used to apply the earthquake.

$$(\mathbf{DI})_{\mathbf{K}} = \mathbf{1} - \frac{\mathbf{K_{final}}}{\mathbf{K_{initial}}} \quad \text{Equation 2-31}$$

Where

$K_{initial}$ = Initial slope of the base shear vs. top deflection relationship resulting from the pushover analysis before the time-history analysis.

K_{final} = Initial slope of the same relationship after the time-history analysis.

According to Kyriakides (2007), following criteria is to be satisfied for selecting a damage indicator to use in a framework.

a. Safety of a damaged structure and Residual strength should be taken as a whole (Global DI).
b. Damage Indicator should be adjusted against recorded data acquired from damaged buildings.
c. Capacity envelope should be associated with DI.
d. Critical damage thresholds such as softening, cracking and yielding due to cumulative and local damage must be considered.

From the above criteria, Kyriakides (2007) concluded that most suitable quantification of damage potential is by a direct relationship with the increase in the natural time period of the structure. This correlation between damage and increase in period is verified experimentally by Calvi et al. (2006). Zembaty et al. (2006) produced a damage scale which defines the structural damage level with the drop of recorded values of natural frequency (Kyriakides, 2007).

$$\mathbf{DI} = \mathbf{100}\left(\frac{\mathbf{T_{sec}} - \mathbf{T_{initial}}}{\mathbf{T_{100}} - \mathbf{T_{initial}}}\right) \quad \text{Equation 2-32}$$

Based on the above proposition, the defined DI is normalized for the initial condition of zero damage at initial period $T_{initial}$

Kyrakidas (2007) used final relationship for the Damage Indicator is standardized for no damage at DI=0 and collapse at DI=100 at each SA_i and SD_i coordinate.

2.5 Summary

In this chapter a discussion on the masonry infills is presented along with the general response of RC frames containing these infills. Different failure modes and the various modeling techniques available in literature for these infills are also discussed in this chapter. Then few analytical models for the shear strength of Reinforced concrete frame members are provided in order to study the behavior of masonry infilled RC framed structures.

In the end a brief discussion on seismic vulnerability assessment is presented. Various aspects and methods for vulnerability assessments are discussed along with the different methodologies and their effectiveness for reinforced concrete structures. Several other aspects of Vulnerability assessment such as selection of analytical tool, capacity models, damage indices etc. are also discussed in this chapter.

Chapter 3

3 EXPERIMENTAL PROGRAM

3.1 Introduction

This chapter presents the experimental testing carried out to determine the compressive strength of masonry required for material modeling of equivalent struts. The testing was conducted to evaluate the compressive strength of typical Pakistani brick masonry. For the preparation of samples, cement-sand mortar and locally manufactured bricks collected from different sources were used.

3.2 Properties of Pakistani Masonry

3.2.1 Masonry Unit

For construction of infill panels in Pakistan, mostly clay bricks and hollow concrete blocks are used. However, only clay bricks are considered in this research.

3.2.1.1 Bricks

The clay bricks are produced manually by pressing clay with small amount of sand in wooden moulds. These wet bricks are dried in sun and air and then they are transported to brick kiln for the subsequent burning process. In the brick kiln they are burnt up to the temperature of 800-900 C^o. Due to the lack of temperature control in kiln, normally three types of bricks are produced. The bricks with sharp edges, good strength and comparatively low absorption are categorized as first class bricks and are recommended for building construction. The porous under burnt bricks with low strength and comparatively high absorption are termed as second class bricks. These bricks are preferably used for small residential buildings and for infill panels. The other brick types with irregular shape which are over burnt and have brownish color are not used for construction purposes (Naseer, 2009).

3.2.2 Mortar

Mortar is used for the bonding masonry units. It is the mixture of bonding material, aggregates and water. Cement and/or lime as a bonding material and sand as aggregates are mostly used. The proportions of constituent materials vary based on the thickness of wall and the purposes of its construction (for load bearing or partitioning). The constituent materials are mixed manually and to achieve the workable paste, water is arbitrary added.

3.3 Testing of Brick Masonry

The following tests were conducted on brick masonry

- Compressive strength of clay bricks
- Compressive strength of mortar
- Compressive strength of masonry assemblages (stacked prisms)

3.3.1 Compressive strength of clay bricks

Compressive strengths of bricks were carried out in compression testing machine in accordance with ASTM C-67 as shown in figure 3.1. According to this standard, “length of test specimen for compressive strength should be equal to one half the full length of the unit ± 1 inch”. However, in this study the compressive strength of full brick was determined. The bricks were capped with gypsum on both sides 24 hours before testing. Bricks were loaded perpendicular to their bed faces (length x width). The compressive strength of bricks is given in Table 3.1.

Figure 3.1: compressive strength test of brick masonry unit.

Table 3.1: compressive strength of brick masonry unit

S. No	Length in (mm)	Width in (mm)	Height in (mm)	Crushing Load (KN)	Compressive Strength (MPa)
1	225	105	70	275.7	11.7
2	226	108	72	272	11.1
3	225	110	69	277.2	11.2
4	221	110	70	202.5	8.3
5	220	105	72	218.4	9.5
6	220	110	70	213	8.8
7	225	108	70	303.2	12.5
8	222	108	70	213	8.9
9	220	110	70	233.8	9.7
10	223	108	70	309	12.8
Average	222.7	108.2	70.3	251.78	10.45

According to the building code of Pakistan (BCP), the minimum compressive strength of brick masonry unit is 8.25 MPa. Tests performed in this research reveal that the compressive strength of bricks complies with BCP.

3.3.2 Compressive strength of Mortar

In this study cement-sand mortar is used. One part cement to four parts sand by volume were proportioned for the mix. Water to cement ratio for workable paste was kept 0.9. Sand from Lawrencepur region was used. The proportion of the mortar selected is representative of the field conditions. The samples of 2 in cube were prepared in mould as shown in figure 3.2 and were cured in water for 7 days and then were stored in moist room until testing day. The specimens were prepared and tested in accordance with ASTM C-109.

Figure 3.2: Preparation of 2 in mortar cubes.

Table 3.2: compressive strength of mortar

S. No	Area (mm^2)	Crushing Load (KN)	Compressive Strength (MPa)
1	2581	13.68	5.3
2	2581	18.58	7.2
3	2581	19.62	7.6
4	2581	17.55	6.8
5	2581	18.36	7.1
Average	2581	17.56	6.8

According to building code of Pakistan (BCP) the compressive strength of mortar in seismic zone 2, 3 and 4 should not be less than 4.1 MPa and not greater than 75 % of the masonry bricks compressive strength. The mortar used in this research satisfies the BCP minimum strength requirement.

3.3.3 Compressive strength of Masonry Assemblages

The compressive strength of brick masonry has been determined by testing brick prisms of 225 x 110 x 260 mm (length x width x height) under uni-axial compression. The mortar joint is 10 to12 mm in thickness. An expert local mason was hired to construct masonry prisms. For achievement of field representative conditions, mixing of materials and wetting of bricks have been done by mason.

Figure 3.3: Preparation of brick masonry prisms.

The masonry prisms were cured and stored in the lab. After 48 hours of the specimens preparation, curing was started. The prisms were wet cured for 7 days and were kept in moisture-tight polythene bags for rest of the time until testing day.

The specimens were capped on both ends with gypsum 24 hours before testing. The testing was done in compression testing machine in the structure laboratory, NUST, Islamabad as shown in figure 3.4. The masonry prisms were sampled and tested in accordance with the ASTM C-1314.

To get the overall displacements of specimens, a rig with two 19 mm thick steel plates was fabricated. Two displacement gauges were connected on each side of the specimen. The plates were lubricated with oil and grease to reduce the confinement effect provided by the friction between steel plates and ends of specimen. The instrumentation is shown in figure 3.5.

The specimens were loaded in compression at an average rate of 2.4 KN/s.

Figure 3.4: compression testing of brick masonry prisms

Figure 3.5: Brick masonry prism in testing rig with displacement gauges.

The stress-strain curves of brick masonry samples in compression and their average are shown in figure 3.6 and figure 3.7 respectively.

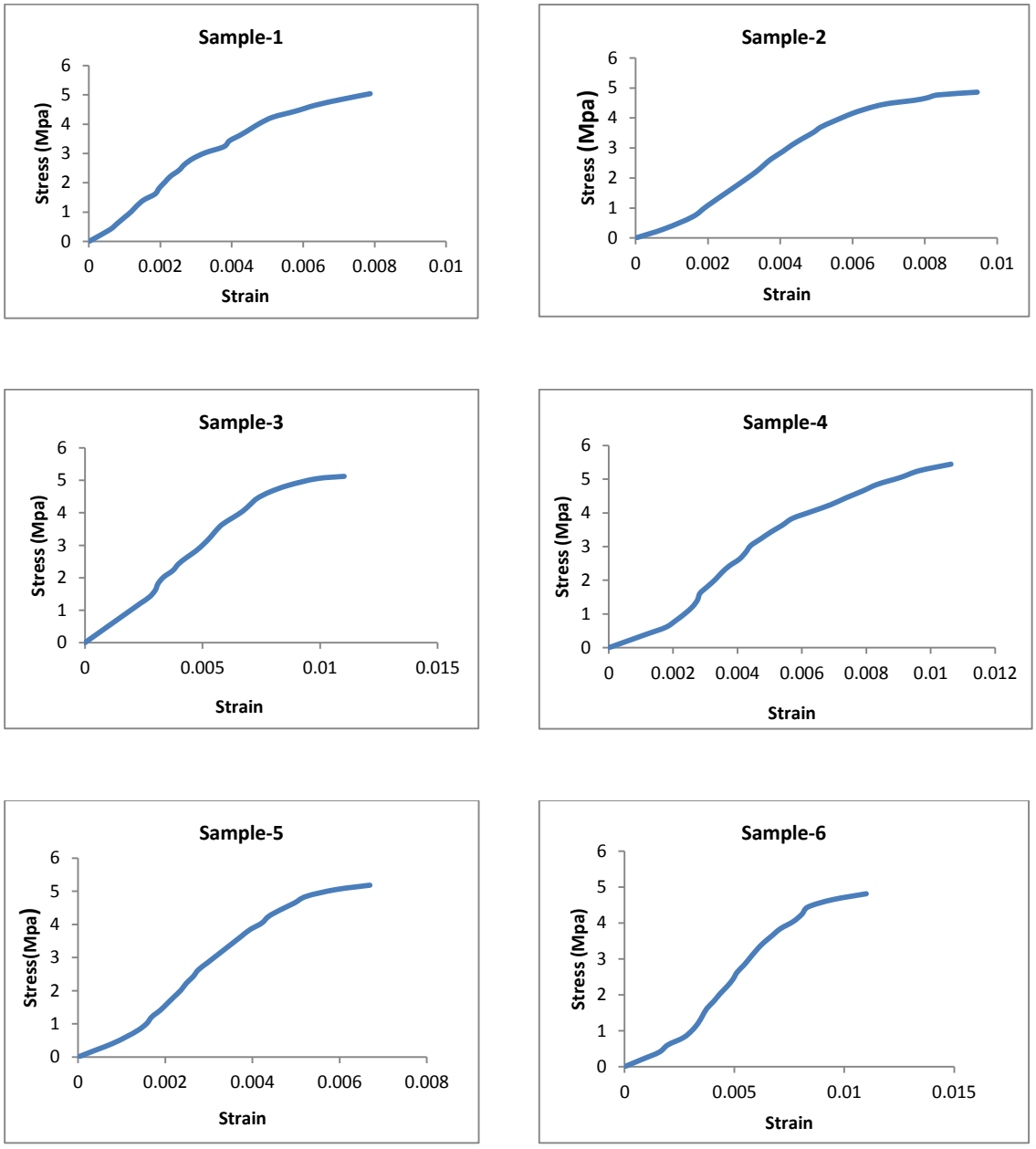

Figure 3.6: Stress-strain curves of few Brick masonry samples in compression.

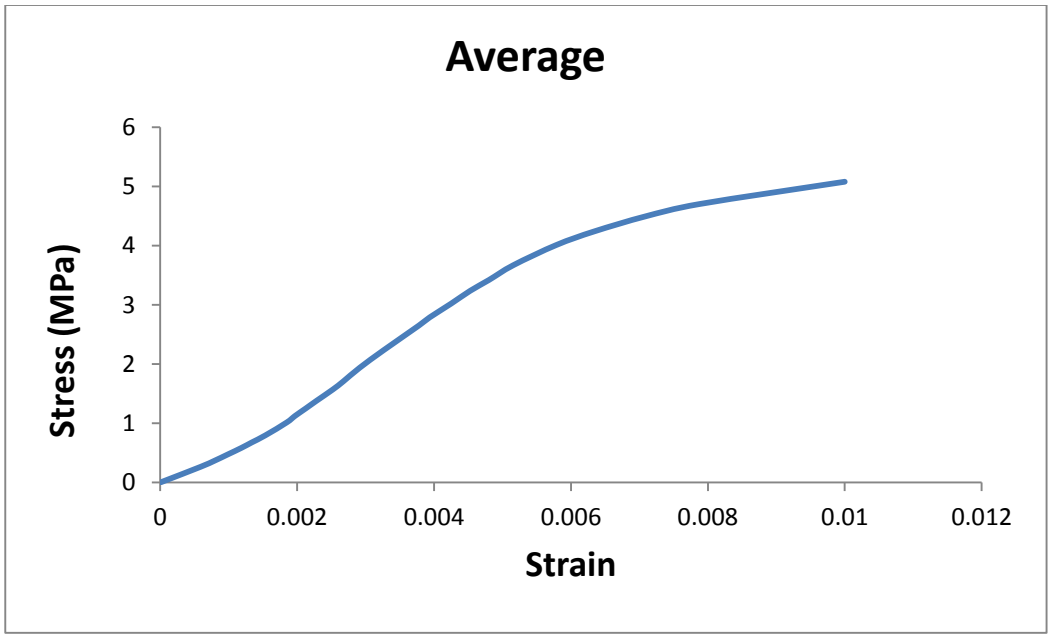

Figure 3.7: Average stress-strain curve of Brick masonry in compression

Table 3.3: compressive strength of masonry prisms

S. No	Area (mm^2)	Crushing Load (KN)	Compressive Strength (MPa)
1	24750	124.7	5.038
2	24750	120.3	4.86
3	24750	126.8	5.12
4	24750	134.8	5.45
5	24750	128.3	5.18
6	24750	119.1	4.81
7	24750	124.3	5.02
8	24750	116.8	4.72
9	24750	131.7	5.32
Average	24750	125.3	**5.06**

3.3.4 Discussion

The stress strain curve obtained from the experimental work is incomplete because the compression testing machine used is stress-controlled which also does not capture the post-peak behavior, hence only peak strength (f'_m) is considered and by using the analytical model, stress-strain behavior of masonry is calculated along the diagonals of infill panels as explained in section 2.2.3.4.

$$f'_m = 5.06 \text{ MPa}$$

3.4 Summary

In this chapter experimental testing of masonry prisms was carried out. The compressive strengths of brick masonry and its constitutive materials i.e. bricks and mortar were calculated experimentally to calculate the compressive strength of Pakistani brick masonry.

Chapter 4

4 STRUCTURAL MODELING

4.1 Introduction

The second chapter discusses the behavior of infilled RC frame structures. The models available in literature for infill panels and shear deformation of critical zones in RC columns were also discussed. In this chapter appropriate models are selected to form finite element model for infilled RC frame structures. The methodology adopted for modeling is also discussed in this chapter.

4.2 Geometry of RC Frame

A two dimensional single bay, two storey frame has been modeled in PERFORM 3D as planer analysis has to be run. The geometrical details of the structure are as follows

- Height of the structure = 6.87 m
- Span length = 4 m
- All columns cross-sections = 260 x 260 mm
- All beams cross-sections = 260 x 400 mm

Reinforcement details of the frame are as follows

- Longitudinal reinforcement
  - 1^{st} storey columns: 3ϕ14 + 4ϕ14 + 3ϕ14
  - 2^{nd} storey columns: 2ϕ14 + 2ϕ14
  - Beams 1^{st} and 2^{nd} storey: 4ϕ14 + 4ϕ14
- Transverse reinforcement
  - Columns: ϕ8mm
  - Beams: ϕ8mm
  - Concrete cover: 30mm from axis of the steel bars

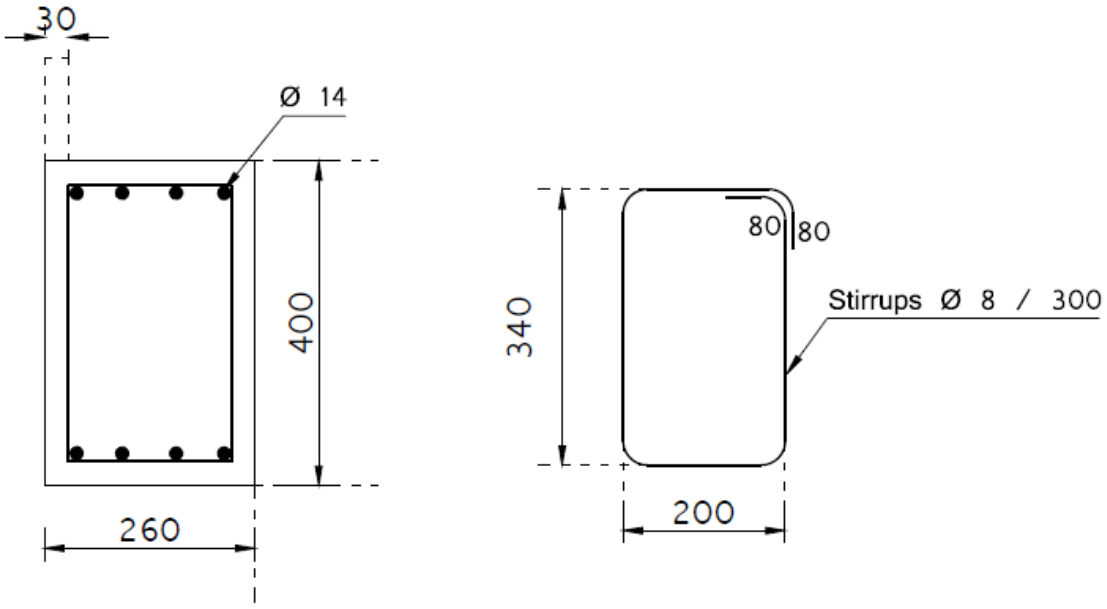

Figure 4.1: Section details of beams

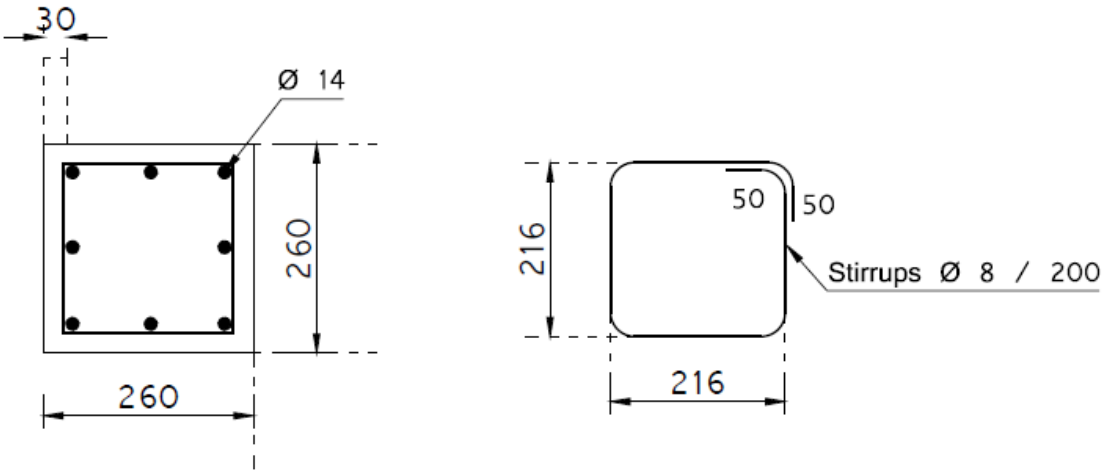

Figure 4.2: Section details of 1st Storey columns

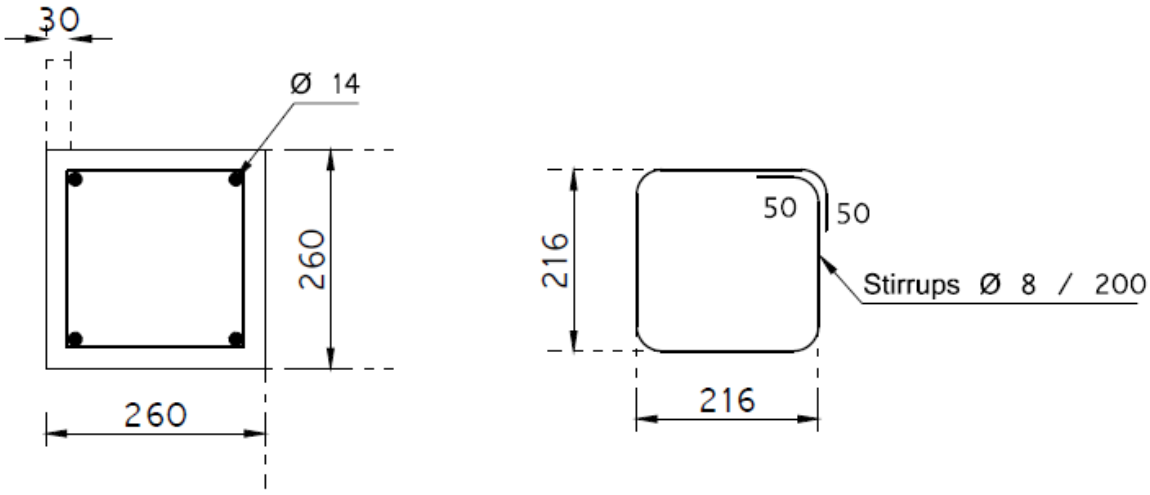

Figure 4.3: Section details of 2nd Storey columns

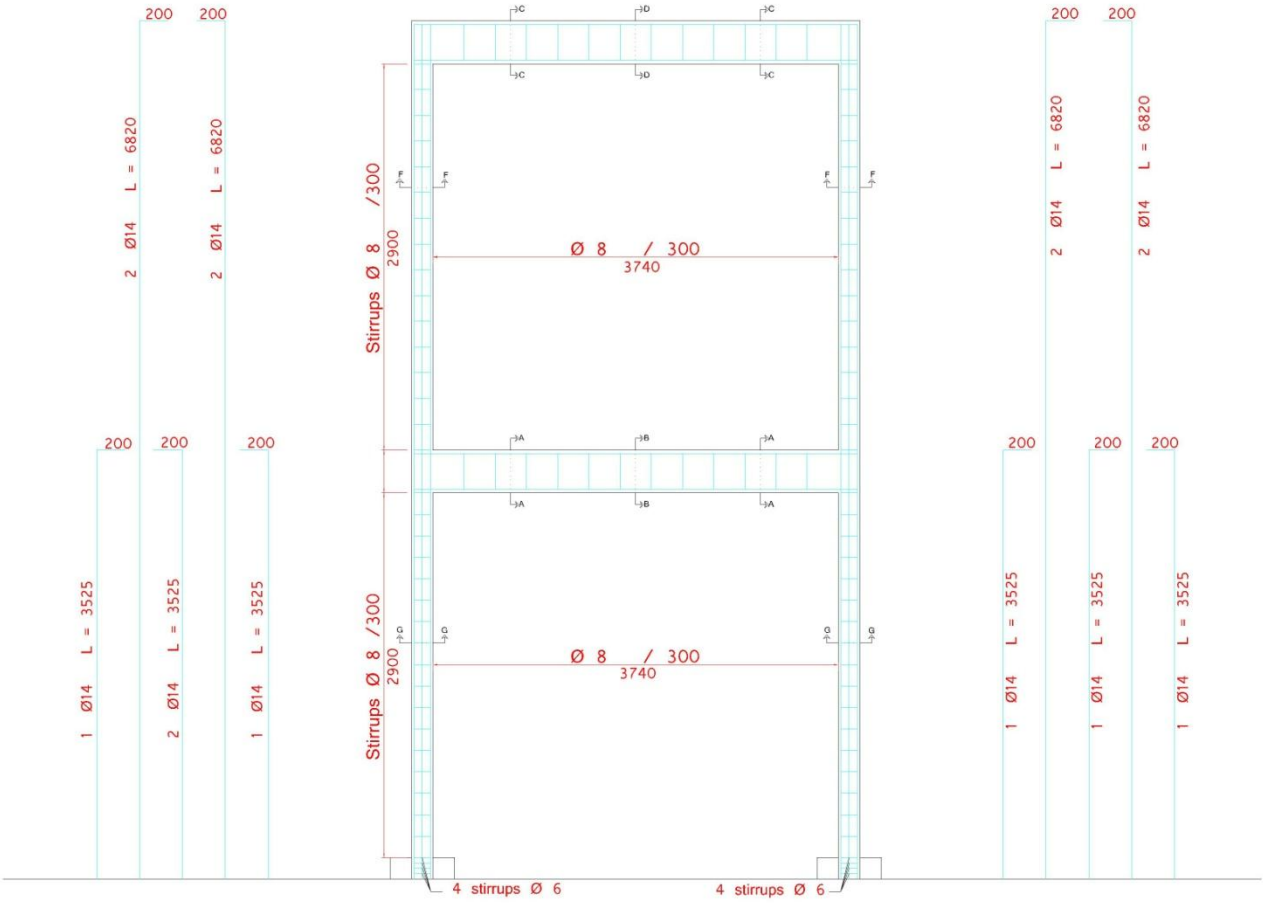

Figure 4.4: Reinforcement details of the structure

4.3 Choice of Analytical Tool

An analytical tool is required for the development of vulnerability curves. PERFORM 3D (2006) is used in this framework for analytical purpose due to availability of many in-built material models and its user friendly graphic interface. Many researchers used PERFORM 3D in their researches like M.N.J Priestley, K Beyer and A Dazio (2008), F Lopez and H Gonzales (2009) and Wen Cheng Liao (2010). Assessment for the performance of structural systems is done by the modeling and analysis in PERFORM 3D. For modeling of the structures, advanced capabilities are provided at the component levels with the force deformation relationships. The further details about PERFORM 3D are given Appendix A.

4.4 Modeling of Infilled RC Frame Structure

4.4.1 Modeling of RC frame

A 2D finite element model is developed as shown in Fig.4.5. Each column and beam is divided into three elements by the addition of intermediate nodes for modeling of masonry struts. To make the frame behave as 2D, restraints are applied at all nodes. All nodes except the foundation nodes are free to translate in H1 or X and V or Y direction and free to rotate in H2 or Z direction. The foundation nodes have fixed supports.

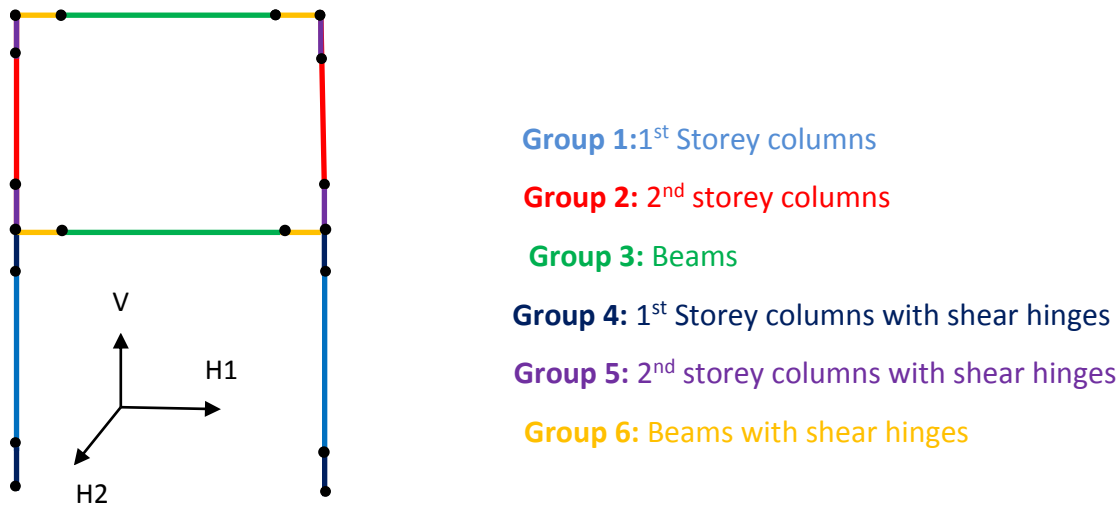

Figure 4.5: 2D Frame model Groups

To model the cross-sections of beams and columns for different stories, the various groups of elements having different compound components are established. For shear behavior of frame members shear hinges are defined which will be discussed in next section. Three groups for frame members with shear hinges are also established. These groups are as follows

Group 1 includes first storey columns with first storey column compound component.

Group 2 includes second storey columns with second storey column compound component.

Group 3 includes beam elements with beams compound component.

Group 4 includes first storey columns with shear hinge and first storey column with shear hinge compound component.

Group 5 includes second storey columns with shear hinge and second storey column with shear hinge compound component.

Group 6 includes beam elements with shear hinge and beams with shear hinge compound component.

4.4.1.1 Material Modeling

For stress-strain relationship of concrete, various models are available in literature as shown in figure 4.6 (a). In this research CEB-FIP Model Code 90 model is used. The stress-strain model from Eurocode is used for steel as shown in figure 4.6 (b). To define the concrete strength in input, five stress-strain points are needed while for steel two points are required. The implemented values of concrete and steel are given in Appendix-B. The figure 4.7 and figure 4.9 shows the models of concrete and steel strength respectively.

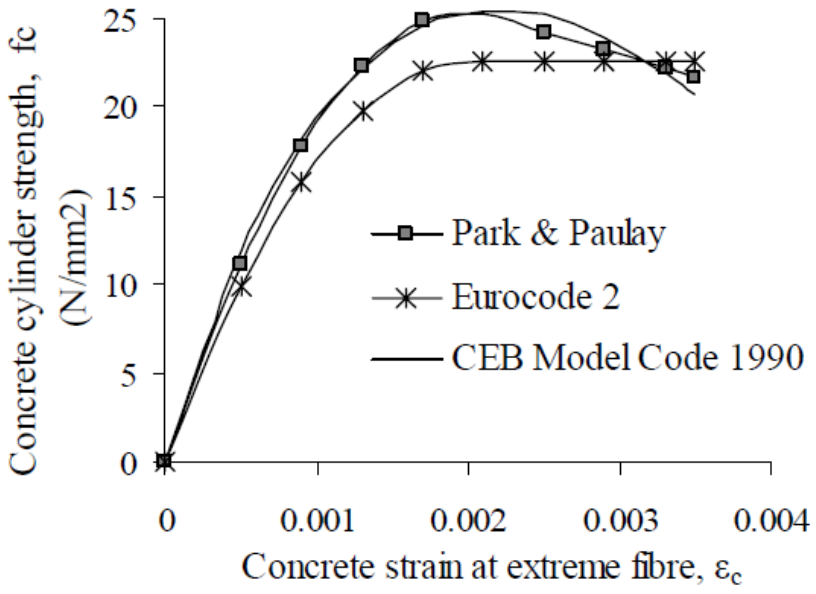

(a)

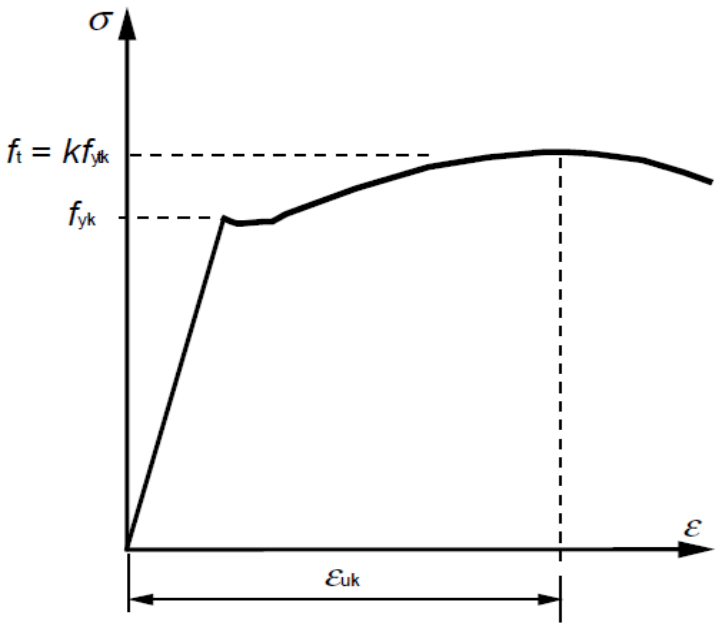

(b)

Figure 4.6: Stress-Strain Models. (a) Concrete. (b) Steel

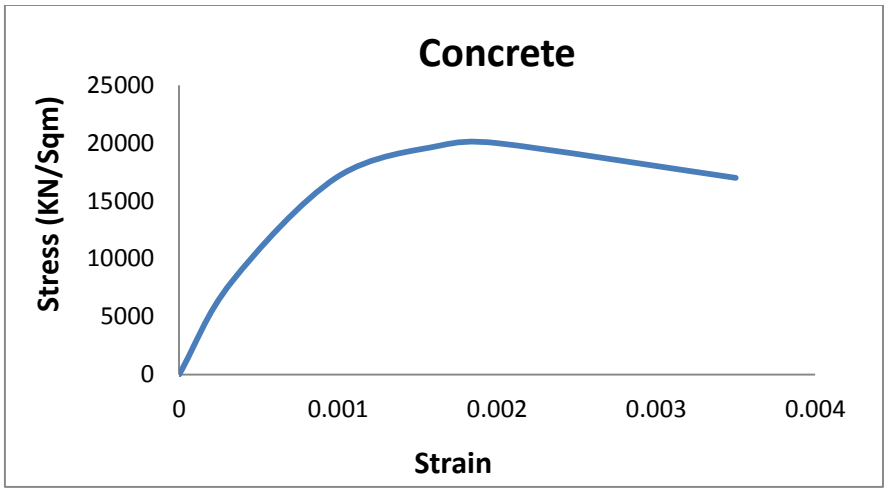

Figure 4.7: Concrete stress-strain model

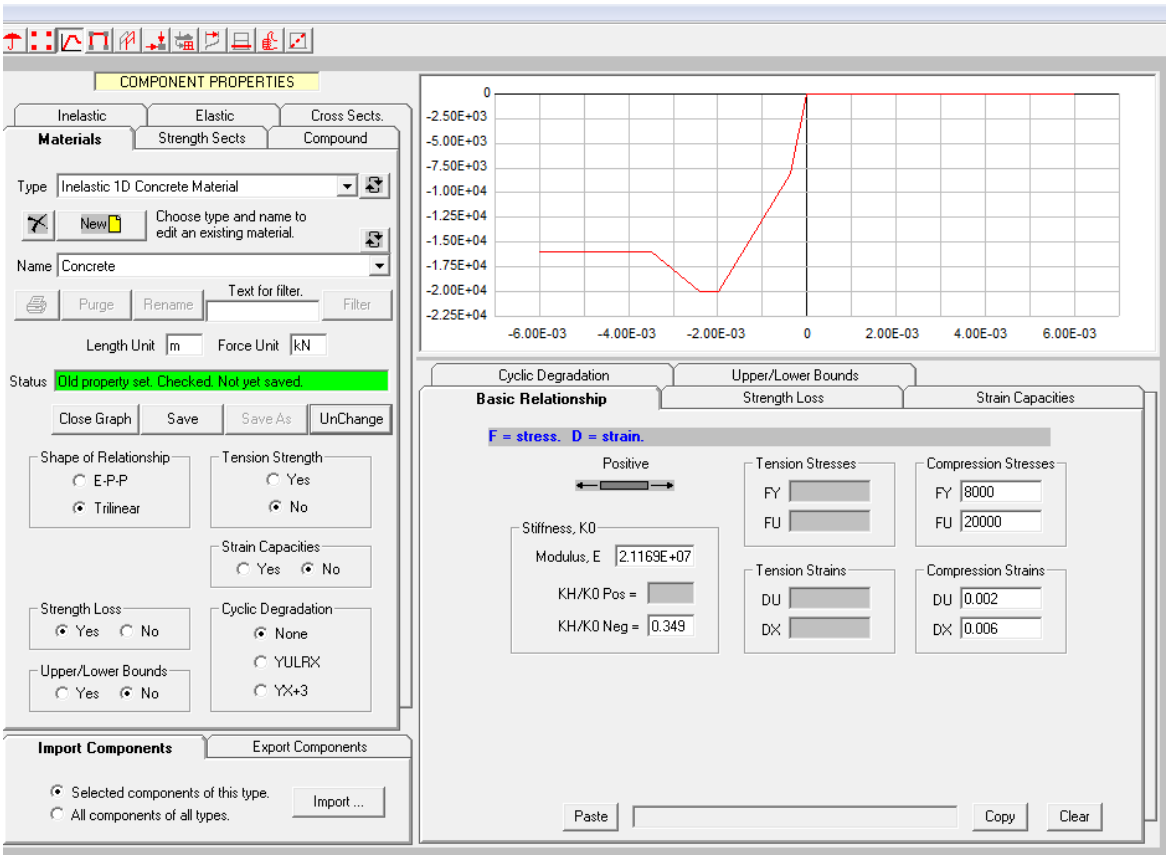

Figure 4.8: Concrete stress-strain relationship in PERFORM 3D

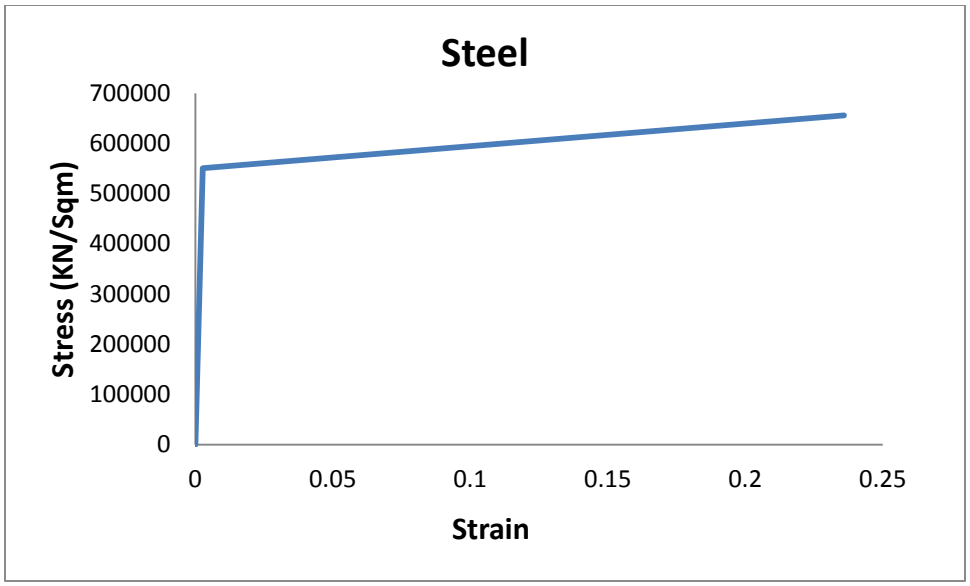

Figure 4.9: Steel strength model

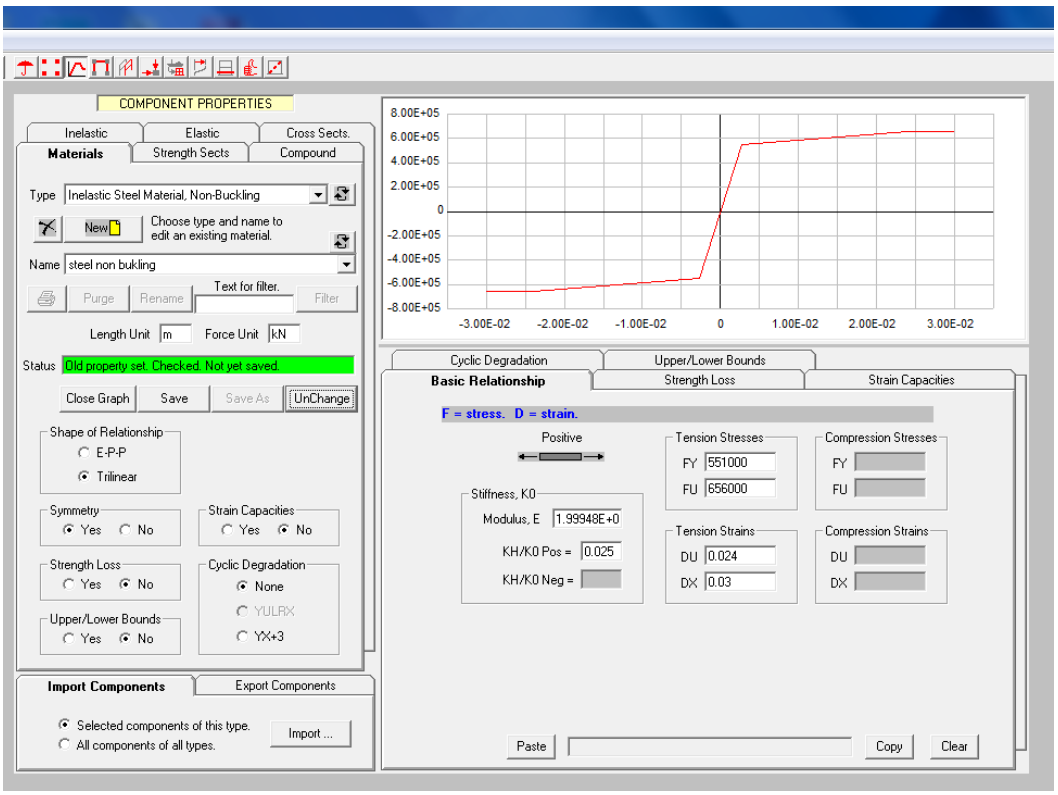

Figure 4.10: Steel stress-strain relationship in PERFORM 3D

4.4.1.2 Beams and Columns Section Definition

For cross section modeling of beams and columns inelastic fiber sections are used. These cross sections are comprised of concrete and steel fibers. The properties of these cross sections are defined by the assembly of these fibers depending on the location (coordinates) of fibers. The centroids of these sections act as the focus of action points for the fibers. The strength and stiffness of the cross sections are dictated by the location and number of fibers (Karman, 2011).

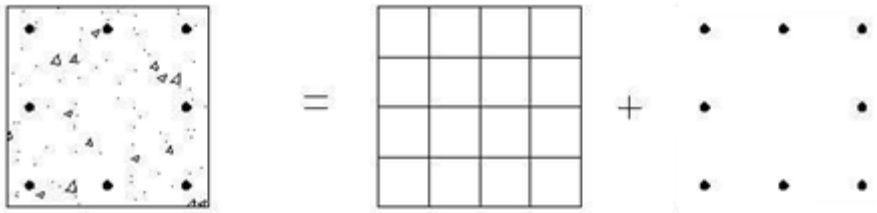

Figure 4.11: Fiber distribution showing concrete and steel fibers.

The cross section of beam is divided into six concrete fibers and four steel fibers at bottom and top as shown in figure 4.12. The required number of fibers for a particular analysis depends on the type of analysis, type of the section and required level of accuracy. Generally the accuracy increases with number of fibers but with increased computational time (user guide, PERFORM 3D).

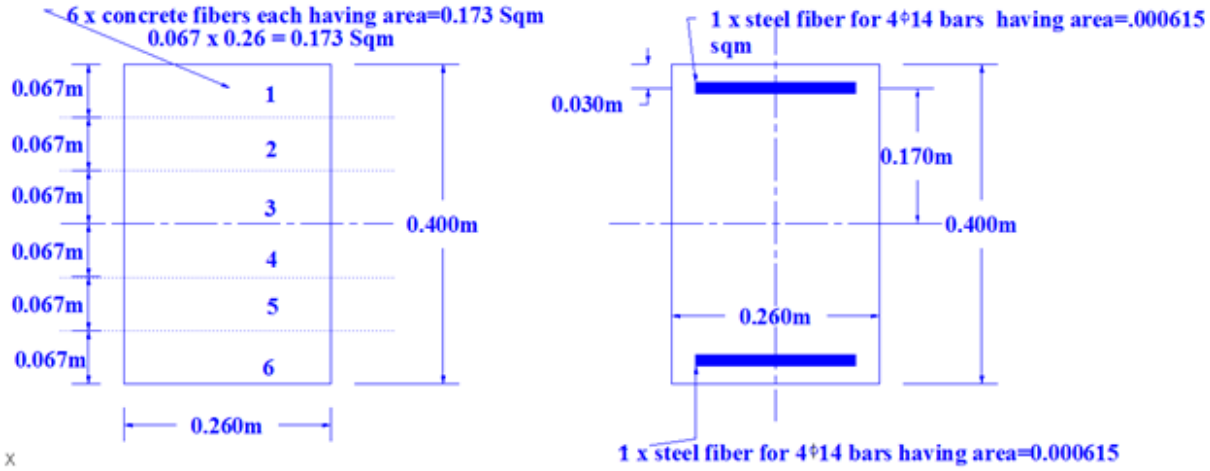

Figure 4.12: Cross-section of beam; concrete fibers (left), Steel Fibers (right).

Similarly, all columns are divided into ten concrete fibers whereas 1st and 2nd storey columns are divided into eight and four steel fibers respectively. The 1st storey columns are shown in figure 4.13 and 2nd storey columns in figure 4.14.

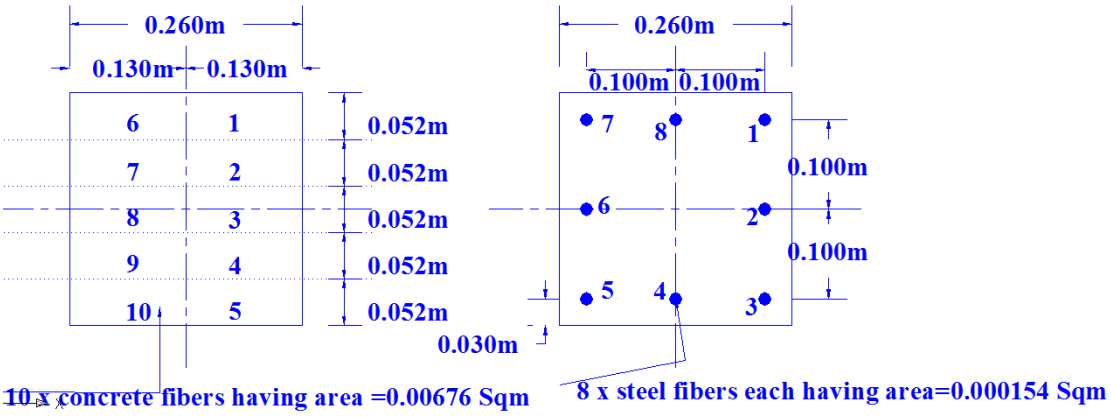

Figure 4.13: Cross-section of 1st storey columns; concrete fibers (left), Steel Fibers (right).

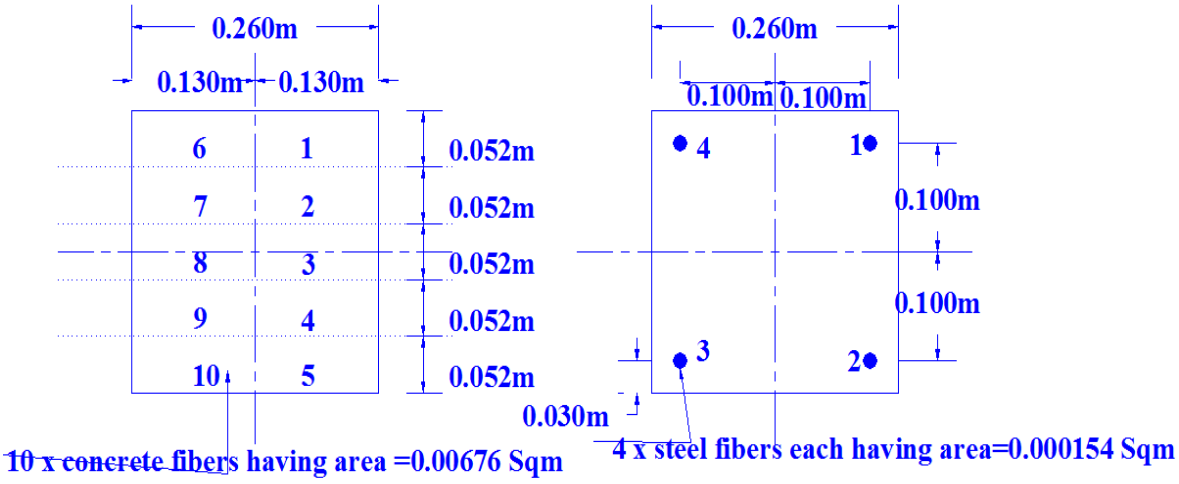

Figure 4.14: Cross-section of 2nd storey columns; concrete fibers (left), Steel Fibers (right).

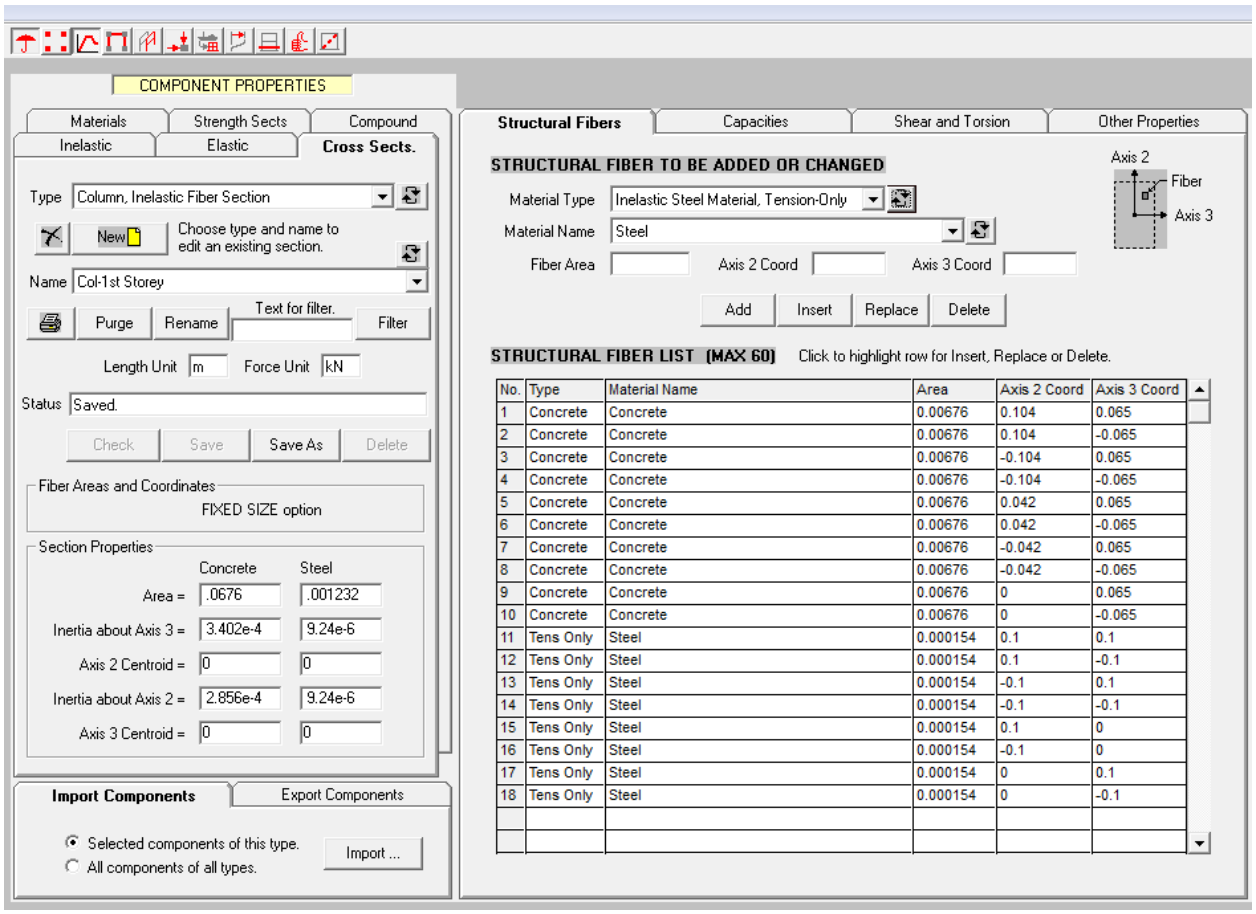

No.	Type	Material Name	Area	Axis 2 Coord	Axis 3 Coord
1	Concrete	Concrete	0.00676	0.104	0.065
2	Concrete	Concrete	0.00676	0.104	-0.065
3	Concrete	Concrete	0.00676	-0.104	0.065
4	Concrete	Concrete	0.00676	-0.104	-0.065
5	Concrete	Concrete	0.00676	0.042	0.065
6	Concrete	Concrete	0.00676	0.042	-0.065
7	Concrete	Concrete	0.00676	-0.042	0.065
8	Concrete	Concrete	0.00676	-0.042	-0.065
9	Concrete	Concrete	0.00676	0	0.065
10	Concrete	Concrete	0.00676	0	-0.065
11	Tens Only	Steel	0.000154	0.1	0.1
12	Tens Only	Steel	0.000154	0.1	-0.1
13	Tens Only	Steel	0.000154	-0.1	0.1
14	Tens Only	Steel	0.000154	-0.1	-0.1
15	Tens Only	Steel	0.000154	0.1	0
16	Tens Only	Steel	0.000154	-0.1	0
17	Tens Only	Steel	0.000154	0	0.1
18	Tens Only	Steel	0.000154	0	-0.1

Figure 4.15: Structural fibers of 1st storey column cross-section in PERFORM 3D.

4.4.2 Modeling of Infill Panels

As discussed earlier in section 2.2.3.3 that three strut models represents the infill-frame interaction more accurately, so a 3-strut model given by Crisafulli (1997) will be employed in this research. The configuration of masonry struts is shown in Fig. 4.16.

To model the infills in PERFORM 3D as inelastic compression struts, the stress-strain relationship is to be defined. Hence, the force-displacement relationship for struts is calculated first using Sattar and Liel (2010) model and then from this F-D relationship stress-strain curve is computed.

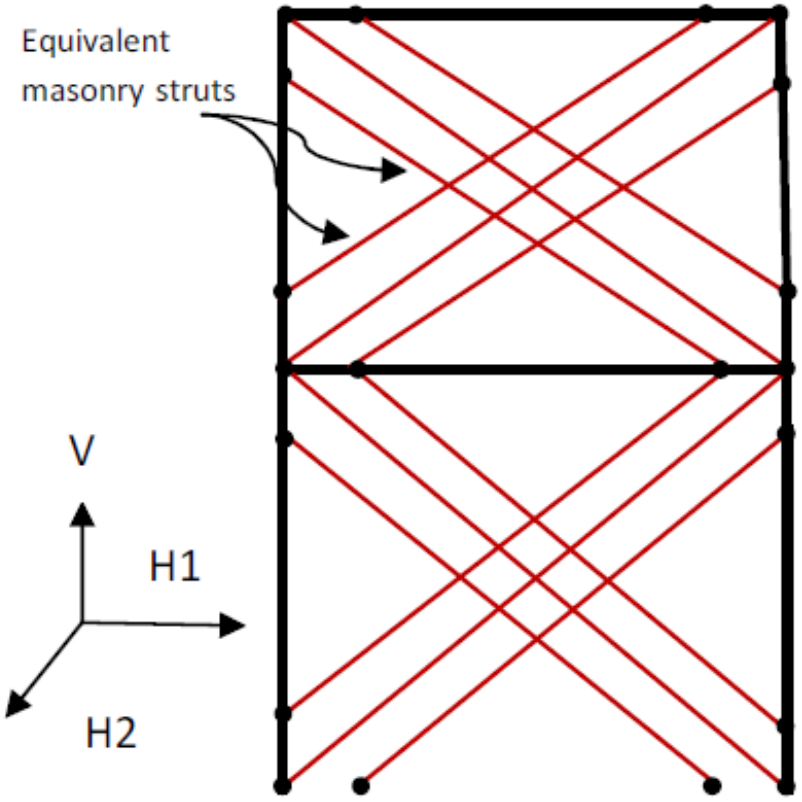

Figure 4.16: RC frame with equivalent masonry struts.

4.4.2.1 Geometrical and Mechanical parameters

To define the behavior of masonry struts, numbers of geometrical and mechanical parameters are required. A list of the variables required as input is presented below along with the recommendations for their values selection. The final implemented values along with the calculations are given in Appendix-B.

Areas of Equivalent Struts

Area of strut is the product of masonry panel thickness and equivalent width of strut. The combine width of all three struts in one direction normally varies from 10% to 25% of the diagonal length of the infill panel. The various expressions for equivalent width are already discussed in section 2.2.3.2.1. In this research the expression given by Paulay and Pristley (1992) is used. Hence, the area of diagonal strut is taken as half of the total strut area in one direction and area of each off-diagonal strut is half of the diagonal strut as suggested by Crisafulli (1997).

Vertical Separation between Struts

Crisafulli (1997) suggested Values for vertical separation as 1/3 to 1/2 of the contact length *z*. The contact length *z* is defined by Stafford Smith (1966), who also introduced the relative stiffness parameter λ. In this research Value of *z*/2 will be used.

$$z = \frac{\pi}{2}.\lambda \qquad \text{Equation 4-1}$$

Where

$$\lambda = \sqrt[4]{\frac{4E_c\, I_c h_w}{E_m t \sin(2\theta)}} \qquad \text{Equation 4-2}$$

The parameters in above equation are already defined in section 2.2.3.2.1.

Compressive strength (f'_m)

It is the compressive stacked prism strength that mainly controls the strut resistance. Prisms are either extracted from masonry walls in field or casted in laboratories. As this research is focused on masonry construction practice in Pakistan, therefore, prisms are casted in laboratory with field representative materials and tested as per ASTM standards. The detailed testing procedure and results are already discussed in chapter 3.

Elastic modulus (E_m)

Elastic modulus (E_m) represents the initial slope of stress-strain curve. Its values exhibit large variations. Many researchers related value of elastic modulus of masonry walls with compressive strength of constitutive materials f'_m. The values proposed by these researchers range between 400 f'_m<E_m<1000 f'_m (Crisafulli, 1997). In this research value of E_m suggested by FEMA 306 and later experimentally verified by Kaushik et al (2007), is adopted.

$$E_m = 550\, f'_m \qquad \text{Equation 4-3}$$

4.4.3 Verification of Strut Behavior

To validate the behavior of nonlinear compression strut element used for modeling of masonry infill panels in PERFORM 3D, a test was performed. A single element was defined and material properties of masonry were assigned to it as shown in Figure 4.18 (a). The compression and tension loads were applied on this element separately and analysis was performed. In tension, no stiffness was exhibited by the strut whereas in compression load strut showed Force-deformation behavior in accordance with the material properties given as input to the element as shown in Figure 4.18 (b). Thus, confirming the nonlinear compression only behavior.

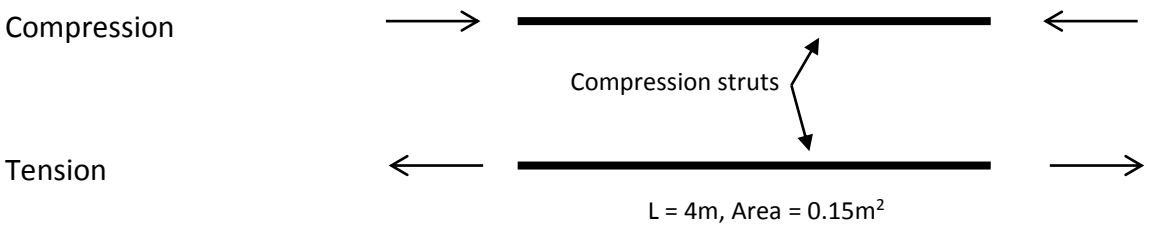

Figure 4.17: Strut element loaded in compression and tension

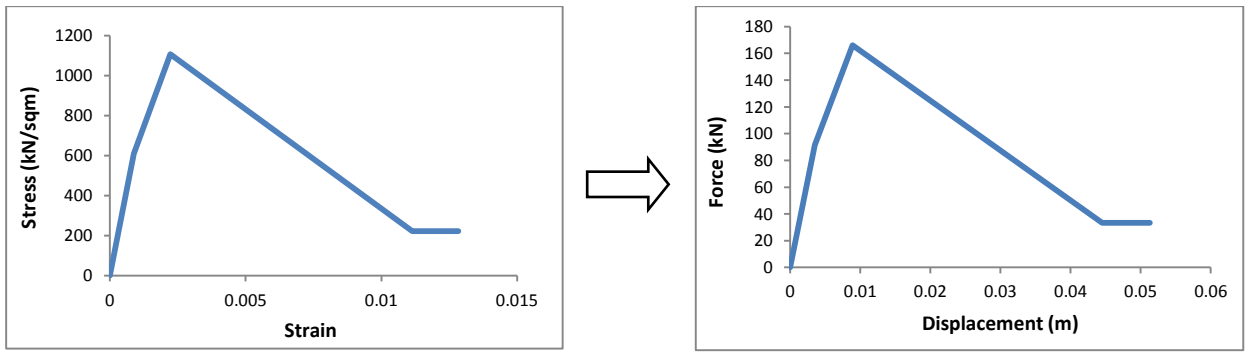

(a) (b)

Figure 4.18: Verification of compression strut behavior (a) Input stress-strain curve for the element (b) Result of load-deformation behavior of the compression strut element.

4.4.4 Modeling of Shear Elements

In PERFORM 3D beam and column sections are both assumed to be elastic for shear and torsion. Therefore, In order to consider the inelastic shear behavior, a shear hinge component is to be used (Components and Elements, PERFORM 3D). In this research work, shear hinges are used at critical locations where inelastic shear behavior is expected i.e. at interaction points of frame members with off-diagonal struts.

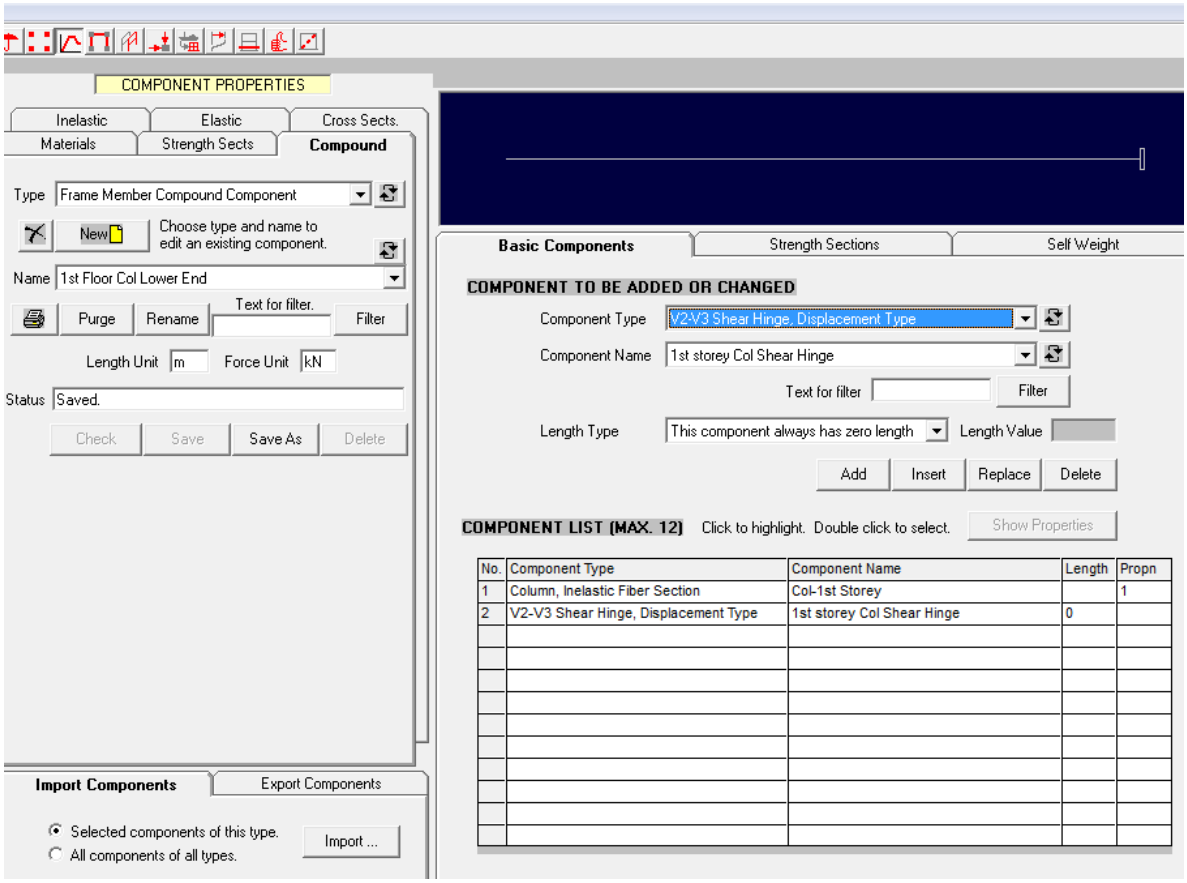

Figure 4.19: Column compound component with shear hinge at one end in PERFORM 3D.

There are two types of shear hinges available in PERFORM 3D i.e. strain hinge and displacement hinge. In strain hinge the action is shear force and the deformation is plastic shear strain while in displacement hinge the action is shear force and the deformation is shear displacement across the hinge. In this framework, displacement type shear hinge is used to

capture the shear behavior of frame members because most of the shear strength models available in literature relate shear capacity of frame members with the displacement ductility which depends on the shear displacement at yield.

As discussed earlier in section 2.3.2 that the shear strength model proposed by Sezen (2002) is more appropriate to be used because of its convenience for modeling in PERFORM 3D. The various equations and their parameters involved in the computation of shear Force-Displacement relationship are already discussed in section 2.3.1.5 and their final implemented values along with the calculations are given in Appendix-B.

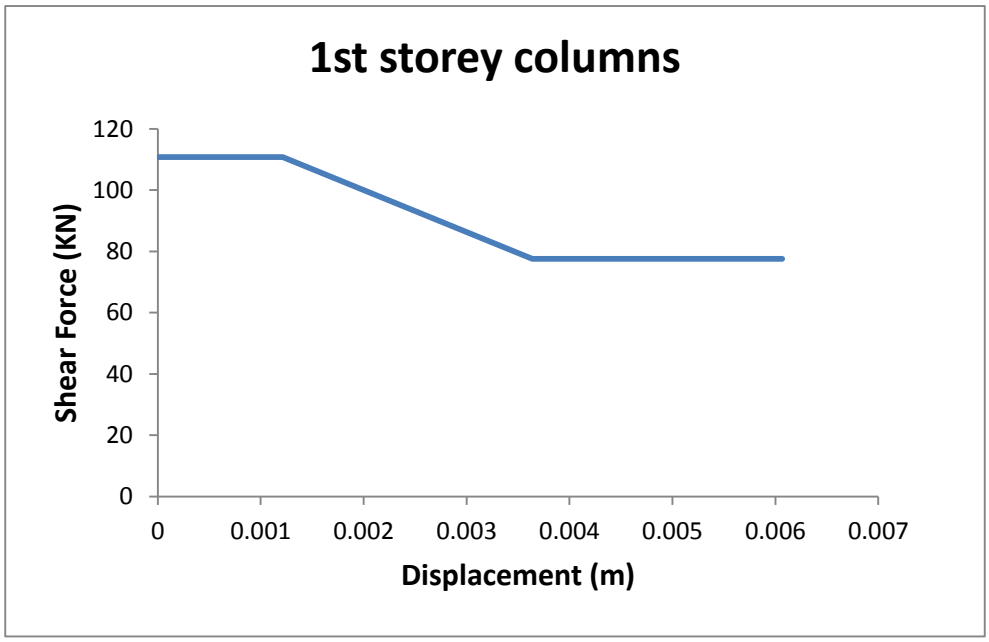

Figure 4.20: Shear force-displacement relationship for 1st storey columns

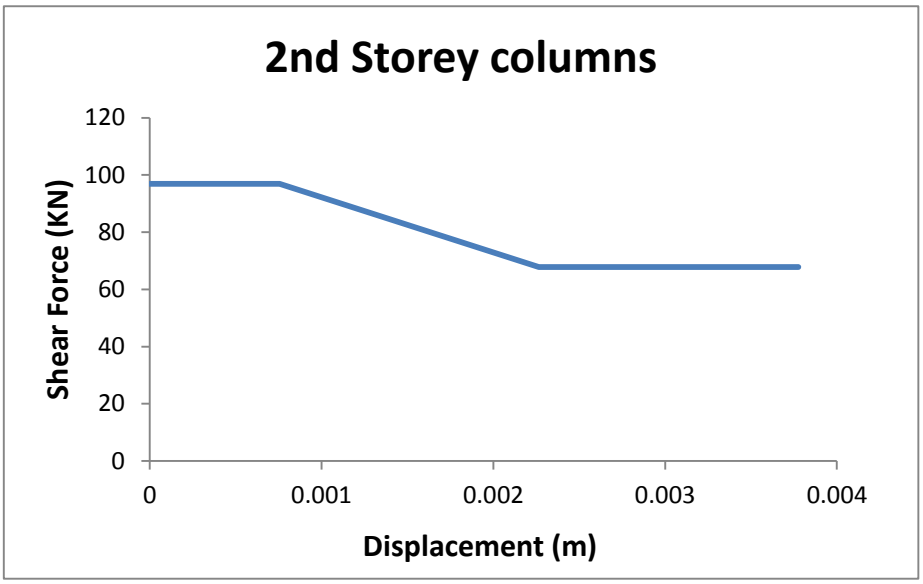

Figure 4.21: Shear force-displacement relationship for 2nd storey columns

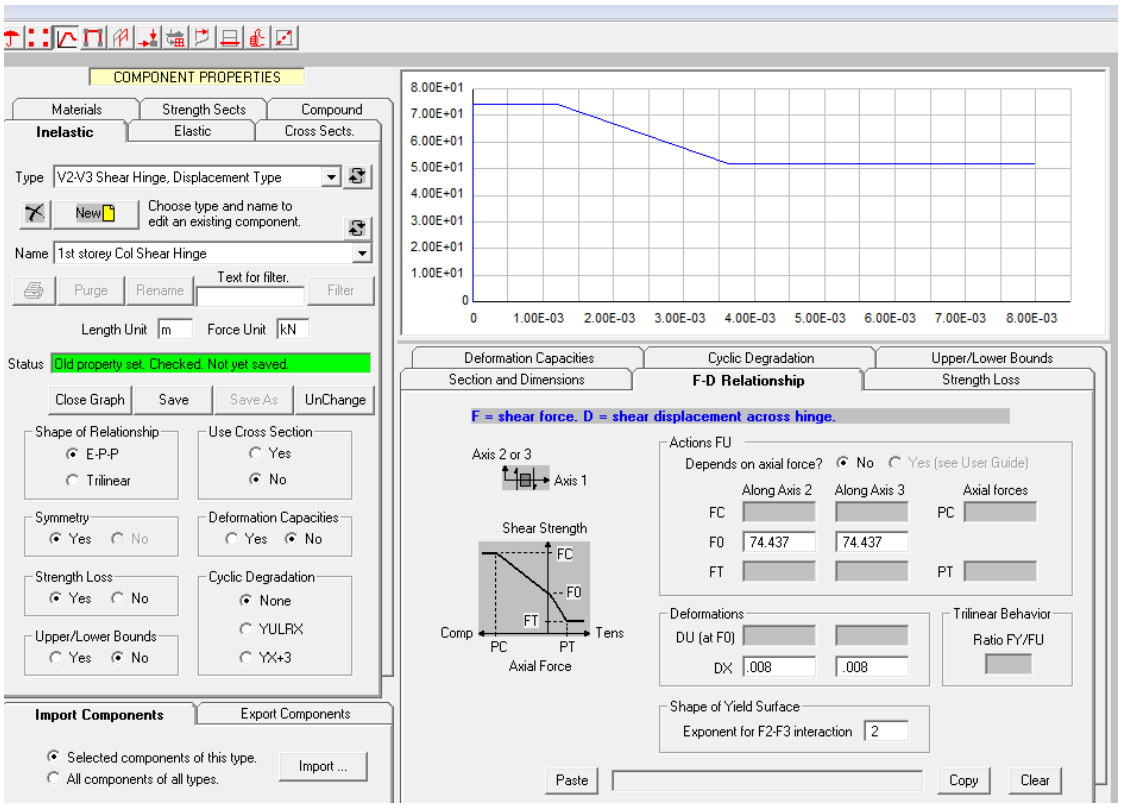

Figure 4.22: F-D relationship for Column shear hinge in PERFORM 3D.

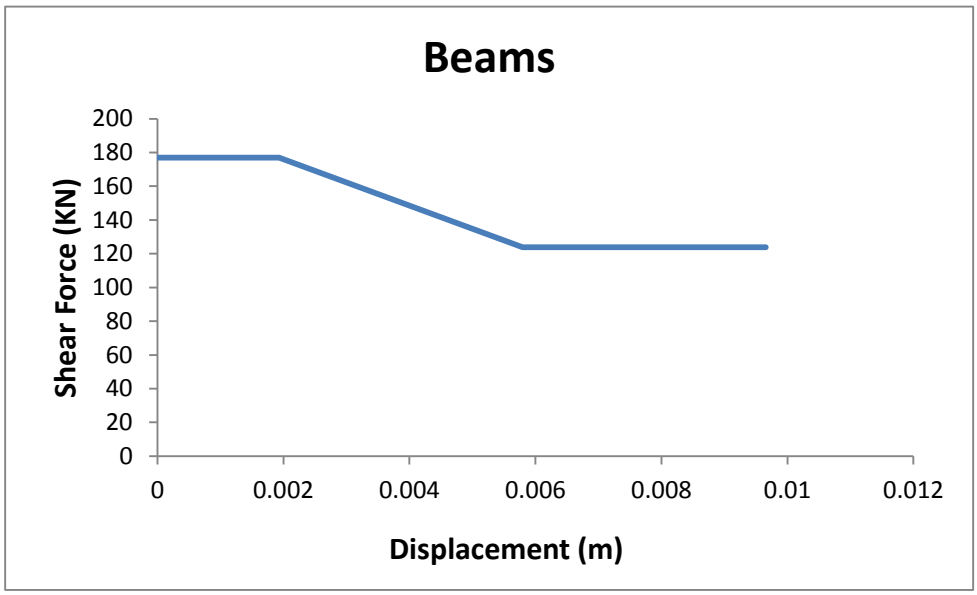

Figure 4.23: Shear force-displacement relationship for Beams

4.5 Summary

In this chapter detailed analytical modeling of infilled RC frame in PERFORM 3D is discussed along with the various models used for materials modeling. The modeling techniques and methodology adopted are also discussed in this chapter.

Chapter 5

5 ANALYSIS, RESULTS AND VULNERABILITY CURVE DERIVATION

5.1 Introduction

This chapter presents the nonlinear static cyclic analysis carried out on RC frame modeled with three equivalent struts as discussed in pervious chapter. Then the results obtained from the analysis in terms of hysteresis loop are discussed. Finally, these results are used to derive the vulnerability curve for masonry infilled RC frame structure.

5.2 Non-linear Static Analysis

Nonlinear static procedures require capacity of a structure to be represented by a capacity curve obtained from non-linear static cyclic analysis. As static cyclic analysis simulates the nature of seismic loading in a better way (Kyriakides, 2007), so for this study non-linear static cyclic analysis shall be used to develop the capacity curve of the structure.

Static cyclic analysis may be performed using a chained sequence of Static analyses, while each Static analysis pushes the structure in opposite direction and would use stiffness from preceding analysis. Each cycle has a specified displacement; lateral loads are applied until that displacement is reached. This specified displacement is increases in each cycle by a displacement step. The displacement steps determine the accuracy of the structure. The smaller the steps, the more accurate results will be, but at the cost of analysis time and increased chance of convergence error. Therefore a suitable value of displacement step is to be selected. Direction of load pattern is reversed after each cycle and the cycles are repeated until desired displacement has been achieved.

The hysteresis loop obtained from static cyclic analysis is shown in figure 5.1(a). The back bone curve of this hysteresis loop is shown in figure 5.2.

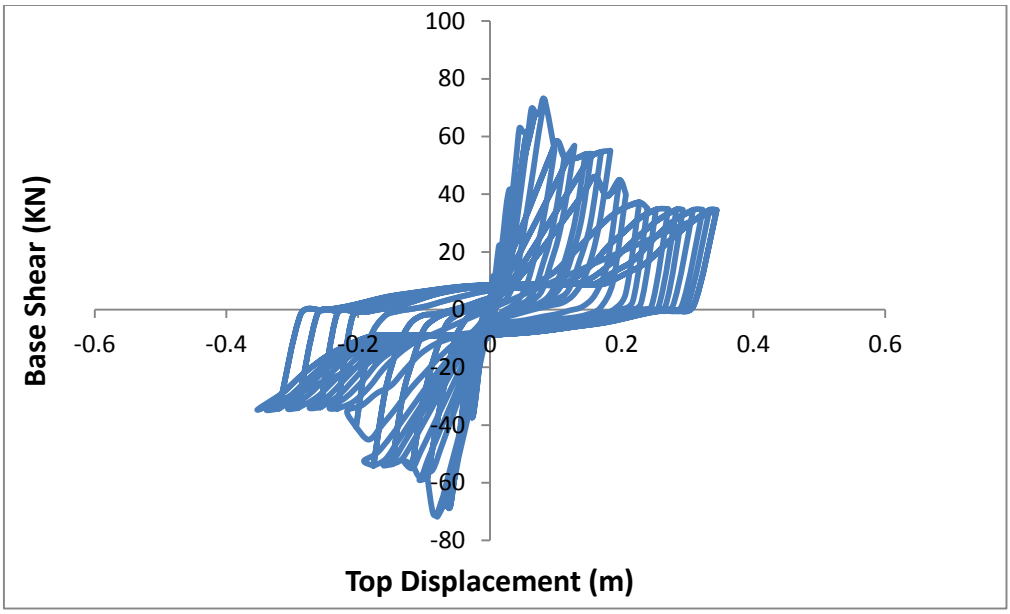

(a)

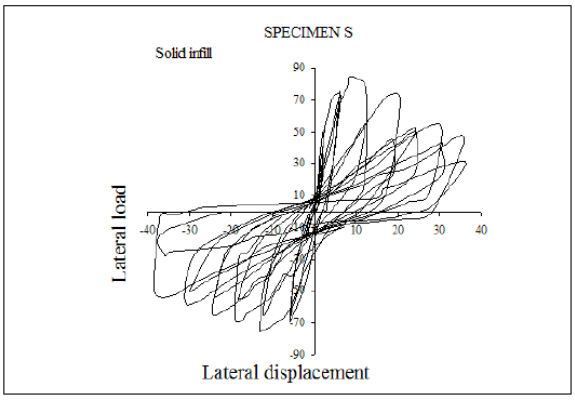

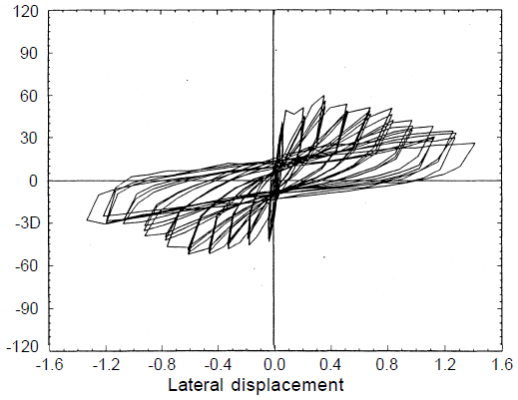

(b) **(c)**

Figure 5.1: Hysteresis loops for Infilled RC frame.

(a) Analytical. (b) Experimental (Karayannis, 2005). (c) Experimental (Mehrabi, 1994)

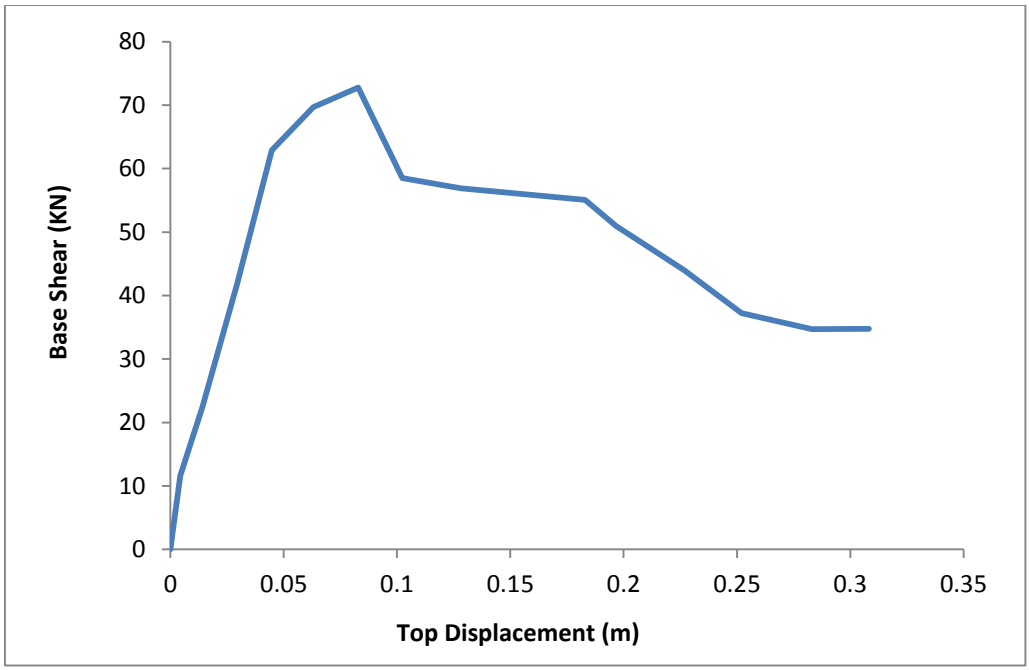

Figure 5.2: Back bone curve for Infilled RC frame

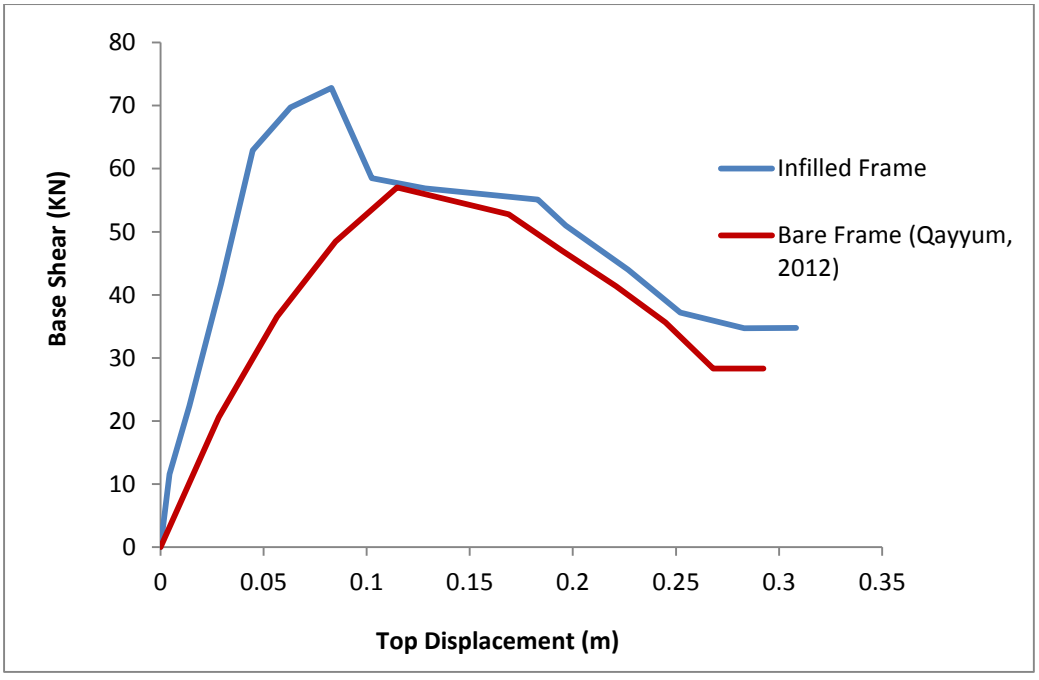

Figure 5.3: Comparison of Infilled RC frame Back bone curve with bare frame.

5.2.1 Discussion

The hysteresis loop obtained from this study was compared with experimental results by Karayannis (2005) and Mehrabi (1994) as shown in figure 5.1. The shape of analytical hysteresis loop of this study resembles the shape of experimental results performed with similar parameters. It is also clear from the Figure 5.1 that both analytical and experimental models show stiffness and strength degradation in a similar manner. Therefore, it is assumed that the analytical model behaves reasonably analogous to the experiment done by Mehrabi (1994) and Karayannis (2005).

The backbone curve of infilled frame obtained from this study was compared with bare frame of Qayyum (2012) as shown in figure 5.3. From the figure it is clear that infilled frame has more stiffness as compared to the bare frame and there is also a brittle failure of masonry at peak value of base shear. After the cracking of infill panel, it still contributes in load resistance to some extent along with frame members.

5.3 Seismic Vulnerability Assessment

As the capacity of building has been evaluated in the form of backbone curve, now the next step is to evaluate the seismic hazards corresponding to various levels of damage in the building. Structural Damage is evaluated against certain displacements which is called damage index. Then for each damage index calculated, a corresponding PGA is calculated representing hazard level. The plot of this is called a vulnerability curve.

In this research work, methodology developed by Kyriakides (2007) for seismic vulnerability is employed, which is a reverse procedure of Capacity Spectrum method (CSM) defined by FEMA 440. The capacity spectrum method (CSM) is a non-linear static analysis method which provides the graphical representation of expected seismic performance of structure. The philosophy behind this method is based on the assumption that the performance of a Multi-degree of freedom (MDOF) system under a specific earthquake event can be

anticipated by comparing the demand from earthquake event with the capacity of an equivalent Single degree of freedom (SDOF) system.

5.3.1 Earthquake Response Spectrum

In capacity spectrum method, the demands imposed by an earthquake event on a structure are represented by earthquake response spectrum. Response Spectrum is essentially a plot of peak response (acceleration, displacement or velocity) with specified damping and varying natural time period, produced by the earthquake's ground motion. For this study, the design spectrum given in UBC-97 shall be used which is also adopted by BCP-2007. This design spectrum depends upon various parameters such as soil type, distance of site from nearest active fault line and earthquake zone.

The design spectrums are prepared according to UBC 97 and assumed soil type for the case building is S_D (Table 16-J, UBC-97) with near source factors equal to one.

$$\boldsymbol{T_0 = 0.2T_s} \qquad \text{Equation 5-1}$$

$$\boldsymbol{T_s = \frac{C_v}{2.5C_a}} \qquad \text{Equation 5-2}$$

Where

C_a = Seismic acceleration coefficient representing design spectrum's PGA, obtained from table 16-Q (UBC-97).

C_v = Seismic velocity coefficient obtained from table 16-R (UBC-97)

Z= seismic zone factor obtained from table 16-I (UBC-97)

The Design spectrum is shown in Figure 5.4.

For the application of capacity spectrum method, the design spectrum is required to be converted into SA-SD space which is termed as Acceleration-displacement response spectrum ADRS (β_0), using the equation of an elastic SDOF system as shown in Figure 5.5.

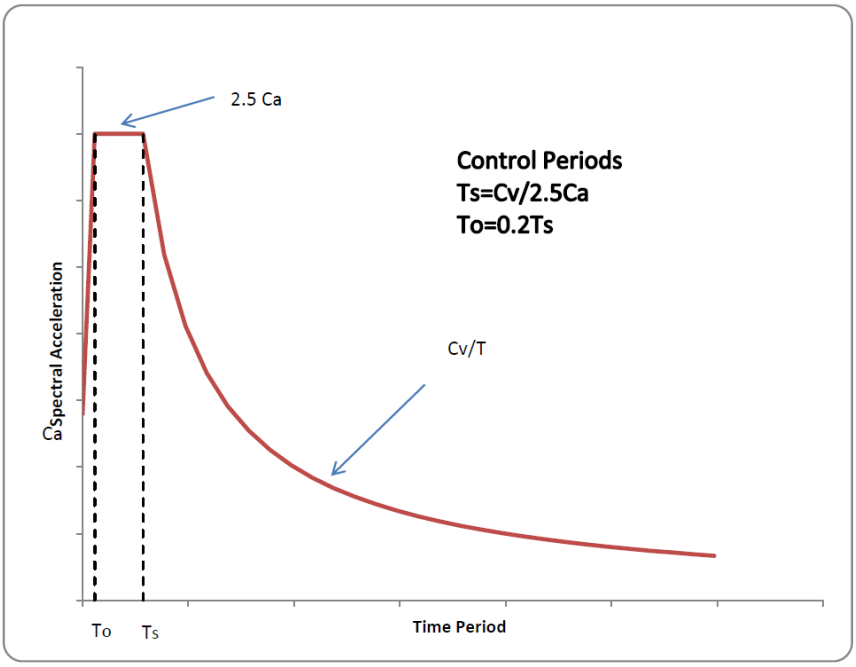

Figure 5.4: UBC-97 Design Spectrum.

$$SD = \left(\frac{T}{2\pi}\right)^2 SA \qquad \text{Equation 5-3}$$

To Ts T To Ts

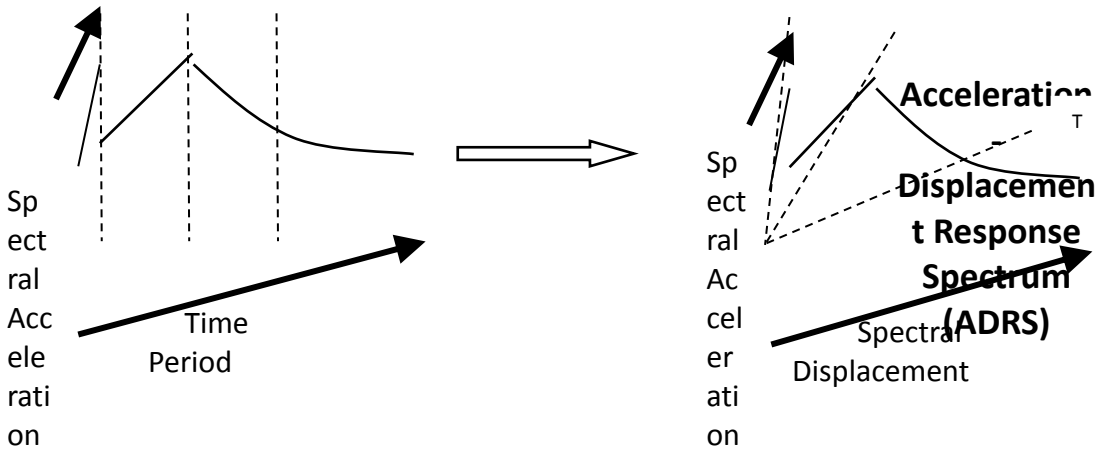

Figure 5.5: Conversion of UBC-97 Design Spectrum into ADRS.

5.3.2 Generation of Capacity Curve

The backbone curve obtained from the static cyclic analysis is representation of capacity of a Multi Degree of Freedom system. To use in CSM, this curve is required to be converted into representative curve of an equivalent SDOF system as shown in figure 5.6. Different methods are available in the literature for this conversion. The ATC-40 method is used for this study, which is also suggested by FEMA 440.

For this conversion, modal participation factor and modal mass coefficient for first mode shape are to be defined. In CSM it is assumed that fundamental mode is sufficient for prediction of response.

$$Modal\ participation\ factor = P.F = \left[\frac{\sum_{i=1}^{N}(w_i\varphi_{i1})/g}{\sum_{i=1}^{N}(w_i{\varphi_{i1}}^2)/g}\right]$$

$$Modal\ mass\ coefficient = \alpha_1 = \frac{[\sum_{i=1}^{N}(w_i\varphi_{i1})/g]^2}{\left[\frac{\sum_{i=1}^{N}w_i}{g}\right][\sum_{i=1}^{N}(w_i{\varphi_{i1}}^2)/g]}$$

Where

Φ_{i1} = amplitude of fundamental (first) mode at level i

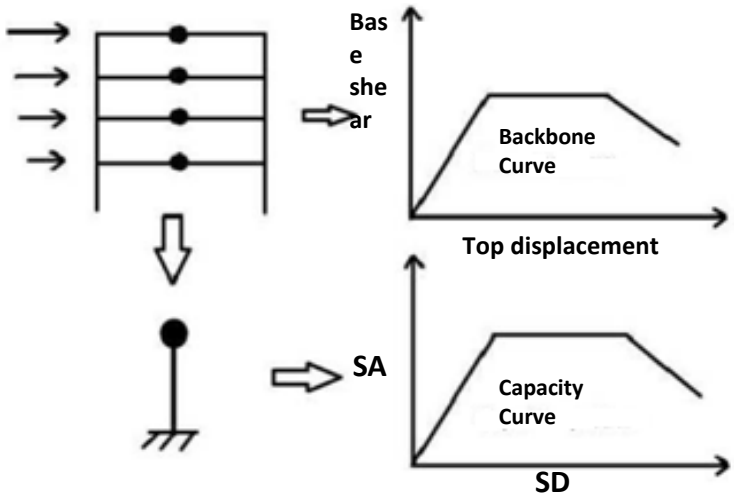

Figure 5.6: Conversion of a MDOF system into an equivalent SDOF system.

The base shear axis of backbone curve is replaced by the spectral axis and acceleration ordinate of Acceleration-displacement response spectrum (ADRS) curve is obtained by the following equation of ATC-40.

$$S_a = \frac{V}{W} / \alpha_1 \qquad \text{Equation 5-4}$$

Where

V = base shear

W_i = seismic weight assigned at level i

The displacement axis of backbone curve is replaced by spectral displacement and is calculated by the following relation:

$$S_d = \frac{\Delta_{roof}}{P.F(\varphi_{roof})} \qquad \text{Equation 5-5}$$

Where

Δ_{roof} = Roof displacement against corresponding V obtained from static analysis.

φ_{roof} = Amplitude of fundamental at the roof, taken as 1 for normalized amplitudes.

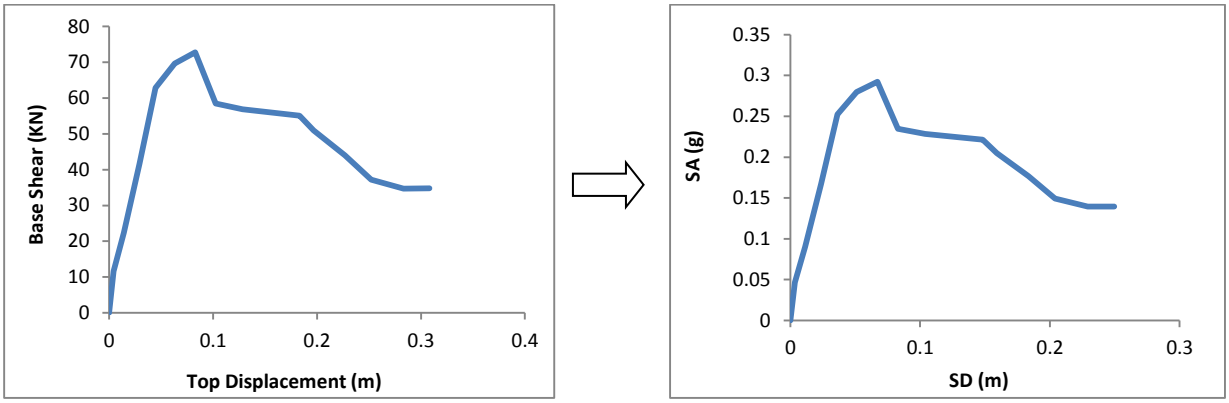

Figure 5.7: Conversion of backbone curve to capacity curve.

5.3.3 Capacity Curve Idealization

To establish the ductility levels for each displacement, the capacity curve needs to be idealized into an elastic perfectly plastic form (Kyriakides, 2007). According to Kyriakides, the idealization of capacity curve with elasto plastic approximation yields inaccurate results for complex degrading behavior of substandard constructions because it is not possible to approximate the ductility at each point on the curve. Therefore, to retain the special characteristics of capacity curve, the shape of curve is approximated with number of different E-P-P systems (considering zero post-yield stiffness).

Each (SD_i, SD_i) point on the capacity curve is chosen and using equal energy rule a bi-linear curve is drawn such that the area under the bi-linear curve and the area above the curve must be equal. However, after degradation the area above the curve (post-yield) is neglected. Figure 5.8 represents a case of this approximation for an assumed performance point. Capacity curve is shown by blue curve while red one is an equivalent E-P-P curve for an assumed PP. yellow color represents the irrecoverable energy due to degradation. Red area under elastic part of equivalent curve corresponds to positive energy which is not dissipated and is balanced by dissipated negative energy in the equivalent system filled with green color.

After the idealization of an assumed performance point on the capacity curve, a corresponding yield point is obtained. The ductility at that point is hence calculated by dividing the displacement co-ordinates of PP with the corresponding co-ordinates of yield point. This process is repeated for every point on the capacity curve. Thus, a single capacity curve is divided into a number of equivalent elastic-perfectly plastic systems.

$$\boldsymbol{\mu = \frac{SD_{pi}}{SD_y}} \qquad \text{Equation 5-6}$$

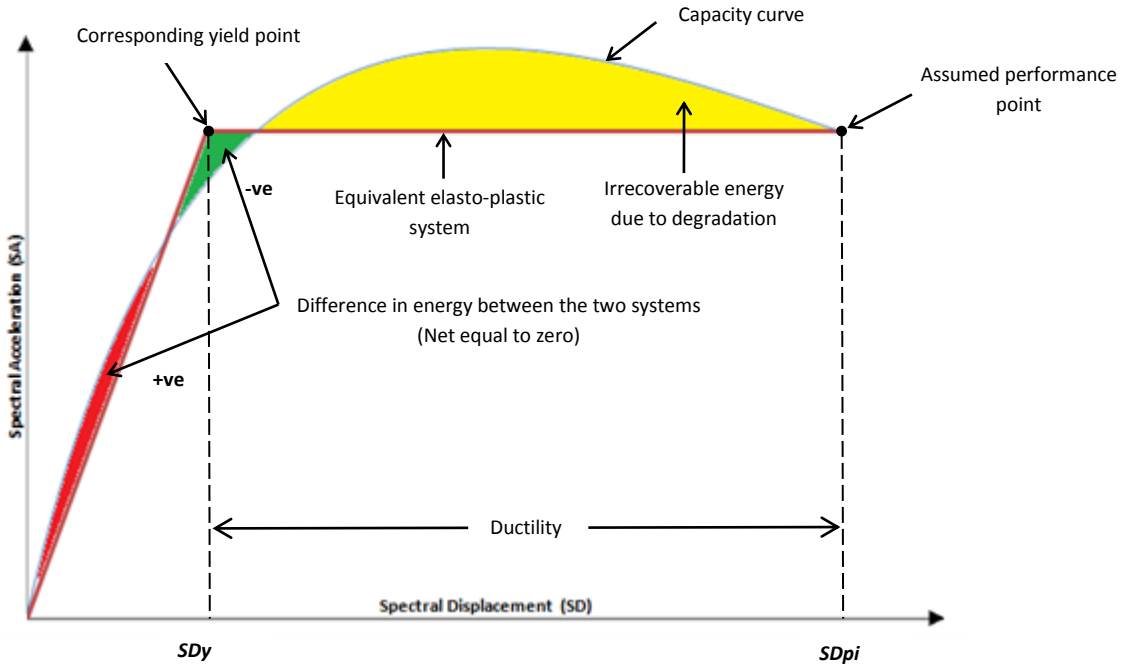

Figure 5.8: Procedure for bi-linear idealization

5.3.4 Capacity Spectrum Method (CSM)

According to FEMA 440, the performance point in CSM is determined by iteration. The displacement response of non-linear SDOF is calculated using an equivalent linear system with effective damping β_{eff} and period T_{eff}. This method is explained in following steps:

- Select an elastic response spectrum and convert into ADRS (β_0) as shown in Figure 5.5.
- Assume a performance point on the capacity curve as shown in Figure 5.8 and calculate its ductility μ and secant period $T_{sec.}$

$$\boldsymbol{T_{sec} = 2\pi\sqrt{\frac{SD_i}{SA_i}}} \qquad \text{Equation 5-7}$$

- Calculate β_{eff} and T_{eff} for the specific ductility levels using the equations of FEMA 440.
- Reduce elastic spectrum ADRS (β_0) by incorporating effective damping to obtain ADRS (β_{eff}), by dividing acceleration ordinate with reduction factor *B*.

$$\boldsymbol{B = \frac{4}{5.6 - ln\beta_{eff}(in\%)}} \qquad \text{Equation 5-8}$$

- Generate Modified Acceleration Displacement Response Spectrum MADRS(β_{eff}, M) to incorporate the non-linearity of the structure by multiplying the acceleration ordinate with reduction factor *M*.

$$\boldsymbol{M = \left(\frac{T_{eff}}{T_{sec}}\right)^2} \qquad \text{Equation 5-9}$$

- The performance point (PP) is obtained by the intersection of MADRS(β_{eff}, M) with the capacity curve. If the estimated PP is within the acceptable limits to assumed one, then it is adopted. Otherwise, this process is repeated using another refined PP.

5.3.5 Application of CSM

For the derivation of vulnerability curve, at every displacement step on the capacity curve, the corresponding hazard level (PGA) is the required output. So, instead of varying performance point to suit the hazard level as mentioned above, the hazard level is varied in accordance with performance points as shown in Figure 5.9. Therefore, the above described method has to be reversed so as to determine hazard level for selected points on the capacity curve (Kyriakides, 2007).

To predict the PGA level that brings the structure at a particular displacement, it is required that all the characterizing parameters of the structural response (capacity curve) should be known at all displacements steps. Every point on the capacity curve is treated as a Performance Point, with known initial period and ductility. Thus, the MADRS method of CSM (as stated above) is reversed for every performance point to calculate the SA ordinates of ADRS (β_0) from respective MADRS(β_{eff}, M) using equation 5-10, instead of calculating MADRS(β_{eff}, M) from ADRS(β_0).

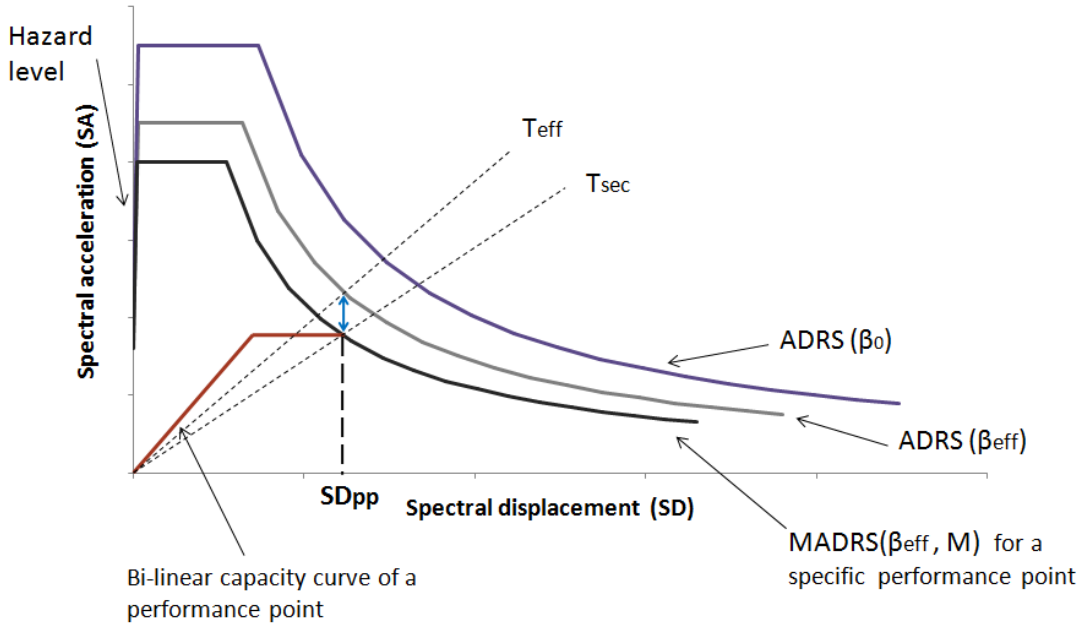

Figure 5.9: Application of CSM for determination of hazard level (PGA).

In above figure, the bi-linear idealized curve of a PP is shown. This point also lies on MADRS(β_{eff}, M) spectrum. The corresponding ADRS(β_0) gives the hazard level (PGA) which brings the structures to this displacement level.

$$SA(ADRS) = \frac{SA(MADRS) * B}{M}$$

Equation 5-10

5.3.6 Quantification of Damage Potential

Quantification of the damage potential at estimated structural response is second task in the derivation of vulnerability curve. In chapter 2 it is discussed that the most suitable quantification of damage potential is by a direct relationship with the increase in the natural time period of the structure because:

- An increase in natural period of structure is a global effect coming forth from localized damage.
- An increase in period can be calculated easily from capacity curve using equation 5-8.
- Any variation in the increasing rate of natural period indicates critical structural damages such as strength loss and yielding.

The damage index (DI) against every PP can be calculated using following relation. At each SA-SD coordinate, the DI is standardized for no damage at the DI=0 and collapse at the DI=100.

$$\mathbf{DI} = \mathbf{100}\left(\frac{\mathbf{T_{sec} - T_{initial}}}{\mathbf{T_{100} - T_{initial}}}\right) \quad \text{Equation 5-11}$$

The time period just before the complete collapse of the structure (T_{100}) is calculated using the guidelines of HAZUS 99. Complete damage is the point at which structure is considered to be collapsed. It is determined by a limiting value of spectral displacement SD_{limit}.

$$\boldsymbol{T_{100} = 2\pi\sqrt{\frac{SD_{limit}}{SA}}} \quad \text{Equation 5-12}$$

For the derivation of Vulnerability curve, DI is to be correlated with Mean Damage Ratio (MDR) which is the ratio of cost of repair to the cost of replacement.

$$\mathbf{MDR} = \boldsymbol{f}\,\mathbf{(DI)} \quad \text{Equation 5-13}$$

Based on the post-earthquake survey damage data from Cyprus for pre-code buildings, Kyriakides (2007) showed that the DI is correlated to the MDR linearly with the correlation coefficient equal to one. Since such type of data is not available for Pakistani buildings and most of the existing buildings are either non-engineered or designed for gravity loads only, therefore, the value of "*f* " adopted by Kyriakides is used. Verification of this assumption should be done in future investigations.

The vulnerability curve for masonry infilled RC frame structures drawn using the above stated methodology is shown in Figure 5.10.

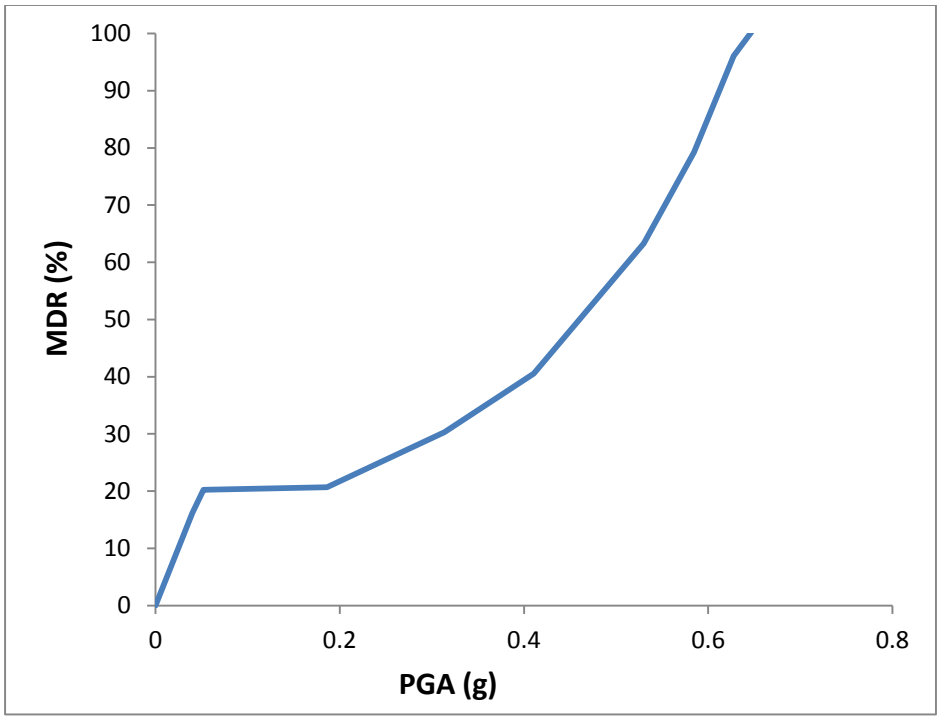

Figure 5.10: Vulnerability curve for infilled RC frame structure

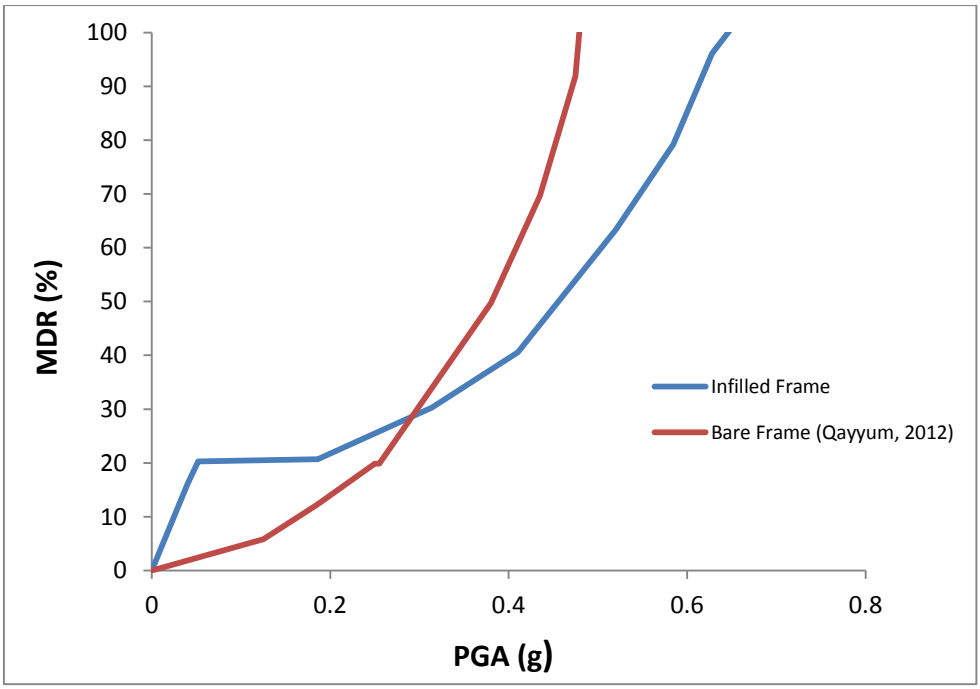

Figure 5.11: Comparison of vulnerability curves developed by Qayyum, 2012 with proposed vulnerability curve in this research work.

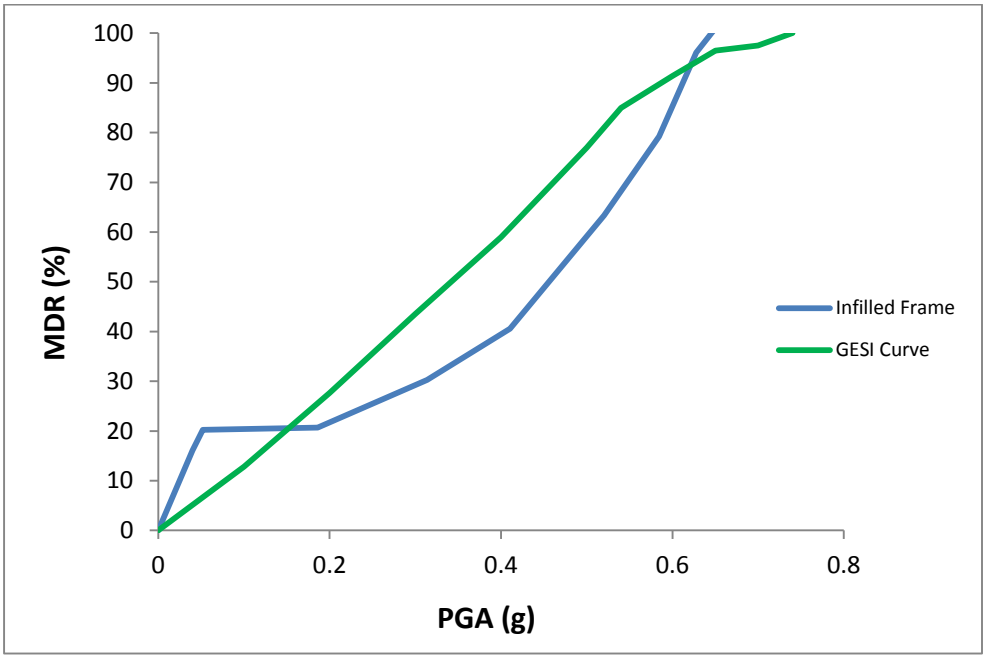

Figure 5.12: Comparison of expert opinion based GESI vulnerability curve with proposed vulnerability curve in this research work.

5.3.7 Discussion

The vulnerability curve obtained from this research was compared with the vulnerability curve of bare frame proposed by Qayyum (2012) with similar parameters and GESI expert opinion based curve as shown in figure 5.11 and figure 5.12 respectively. From comparison of these vulnerability curves it is clear that the structures with masonry infills can withstand higher PGA as compared to the bare frames prior to their failure but they are more vulnerable below 0.3g (lower values of PGA). This phenomenon verifies the viewpoint present in literature (as discussed in section 2.2) that initially masonry infills resist the forces induced by earthquake loading whereas RC frame is critical for the performance of the structure at stronger excitations and presence of masonry infill panels enhances the overall seismic response of the RC structures.

The GESI expert opinion based vulnerability curve (as discussed in section 2.4.1.2) is used by many researchers in Earthquake risk assessment (ERA). This curve does not incorporate

the brittle failure mode of masonry infill panels. From the Figure 5.12 it is clear that the linear GESI curve does not depict the actual behavior of masonry infilled RC frame structures as it underestimates the damage in masonry panels below 0.2g and overestimates the damage at higher PGA levels.

Summary

In this chapter the nonlinear static cyclic analysis carried out on RC frame modeled with three equivalent struts is presented. Then the results obtained from the analysis in terms of hysteresis loop are discussed. These results are used to derive the vulnerability curve for masonry infilled RC frame structure. Finally the vulnerability curve obtained from this study is compared with the vulnerability curves of other researchers. From the comparison it was observed that the masonry infilled structures give overall better seismic performance than bare frame structures.

Chapter 6

6 CONCLUSIONS AND RECOMMENDATIONS

6.1 Summary and Conclusions

This study provides a framework to develop the vulnerability curves for masonry infilled reinforced concrete frame structures. The general response of masonry infills in RC frame structures was discussed along with their different failure modes and various techniques used during last few decades for the analytical modeling of infills. The equivalent three struts model presented by Crisafulli (1997) was adopted for infill panels modeling. As this research was focused on Pakistani buildings, therefore, testing was conducted to evaluate the compressive strength of typical Pakistani brick masonry required for material modeling of equivalent struts. The stress-strain behavior of masonry panels along their diagonals was defined by using compressive strength from experimentation and the analytical model proposed by Sattar and Liel (2010). After that few analytical models for the shear strength of Reinforced concrete frame members were provided in order to study the inelastic shear deformation of critical zones in RC columns. Shear strength model proposed by Sezen (2002) was adopted for shear force-deformation of frame members.

A two dimensional single bay, two storey frame was modeled in analytical tool (PERFORMED 3D) with three equivalent struts in each direction. After the modeling, non-linear static cyclic analysis was carried out and the hysteresis loop obtained was compared with the other experimentally obtained hysteresis loops investigated by Karayannis (2005) and Mehrabi (1994). As the hysteresis loops of both analytical and experimental structures were found somewhat similar so, the backbone curve was calculated.

Finally a discussion on seismic vulnerability assessment was presented. Different aspects and methods for vulnerability assessments were discussed along with their merits and demerits. Various methodologies and their effectiveness for reinforced concrete structures

were also discussed and extensively used analytical vulnerability assessment method was selected. Based on the capacity curve obtained from backbone curve, vulnerability curve for masonry infilled RC frame structures was derived using the reverse procedure proposed by Kyriakides (2007) and was compared with that of bare frame derived by Qayyum (2012) and GESI expert opinion based curve.

The conclusions drawn from this research are as follows:

- The vulnerability curve is developed for typical Pakistani infilled RC frame structures showing collapse condition at PGA equal to 0.64g.
- At lower seismic excitations (below 0.3g), the masonry infilled structures are more vulnerable as compared to bare frame structures.
- When compared with bare frame structure, the masonry infilled structure exhibited 100% damage at 38% higher PGA level.

6.2 Recommendations for Future Works

- In this study only in-plane actions of seismic forces are considered. The out-of-plane actions should be considered in the future investigations.
- The framework of this study should be used for various configurations of infills and infill frames to obtain more representative curves for such structures.
- Experimental work should be done on full scale infilled RC structures representing Pakistani building stock to validate the frame work for seismic vulnerability assessment.

REFERENCES

- Ahmad, N. (2008) Development of a Seismic Risk/Loss Model for Mansehra City, Pakistan. Istituto Univeritario di Studi Superiori.
- Amjad Naseer (2009). Performance Behavior of Confined Brick Masonry Buildings under Seismic Demand. Peshawar Department of Civil Engineering, N-W.F.P. University of Engineering and Technology, Peshawar, Pakistan, 2009.
- ATC 40 Applied Technology Council (1996) Seismic evaluation and retrofit of concrete buildings, Publication of the Applied Technology Council, Redwood City, California.
- Bin Zhang. (2006). Parametric Study on the Influence of Infills on the Displacement Capacity of RC Frames for Earthquake Loss Estimation. Master thesis, European School for Advance Studies in Reduction of Seismic Risk, ROSE SCHOOL, Pavia, Italy.
- Calvi G.M., Pinho, R., Magenes, G., Bommer, J.J., Restrepo-Vélez, L.F. and Crowley, H. (2006) Development of seismic vulnerability assessment methodologies over the past 30 years. ISET Journal of Earthquake Technology, 43(3), pp. 75-104.
- Chatzicharalampous, C. (n.d) Vulnerability Curves for the Seismic Assessment of Reinforced Concrete Structures. London: UCL Department of Civil, Environmental and Geomatic Engineering.
- Chopra, A. K., 1995. Dynamics of Structures – Theory and Applications to Earthquake Engineering. Prentice Hall of India.
- Chrysostomou, C. Z., Gergely, P., and Abel, J. F. (2002). "A six-strut model for nonlinear dynamic analysis of steel infilled frames." Int. J. Struct. Stab. Dyn., 2(3), 335–353.
- Comartin, C.G. (1996) Seismic evaluation and retrofit of concrete buildings. California: Applied Technology Council.
- Crisafulli, F. G. (1997). "Seismic behavior of reinforced concrete structures with masonry infills." Ph.D. thesis, Univ. of Canterbury, Christchurch, New Zealand.
- Dincel construction system (n.d.). The roles of Masonry infill walls in an earthquake. Paramatta.

- Ellul, F. and D'Ayala, D., July 2003. "Field Report on the Bingol, Turkey Earthquake of the 1st of May 2003". University of BATH - Architecture & Civil Engineering Department.
- Fajfar P. (1999) Capacity spectrum method based on inelastic demand spectra, Earthquake Engineering & Structural Dynamics, 28, 979-993.
- FEMA 306 (1998) Evaluation of Earthquake Damaged Concrete and Masonry wall buildings. Federal Emergency Management Agency, Washington, D.C., 2000.
- FEMA 440 (2005) Improvement of nonlinear static seismic analysis procedures, Applied Technology Council (ATC-55 Project), Redwood City, California.
- FEMA-273. (1997). NEHRP guidelines for the seismic rehabilitation of buildings. Washington, D.C.
- Freeman, S.A. (n.d) The capacity spectrum method as a tool for seismic design. Elstner associates.
- Government of Islamic Republic of Pakistan Ministry Of Housing And Works (2007) Building code of Pakistan. Islamabad.
- Hassan Ali. (2009). Half Scale Three-Storey Infilled RC Building; A Comparison of Experimental and Numerical Models. Master thesis, European School for Advance Studies in Reduction of Seismic Risk, ROSE SCHOOL, Pavia, Italy.
- Hemant B. Kaushik (2007). Stress-Strain Characteristics of Clay Brick Masonry under Uniaxial Compression. Journal of materials in civil engineering ASCE / September 2007.
- Hemant B. Kaushik, Durgesh C. Rai and Sudhir K. Jain VOL. 92, NO. 4, 25 (2007) Uniaxial compressive stress–strain model for clay brick masonry.
- Javed, M. (2009) Seismic Risk Assessment of Unreinforced Brick Masonry Buildings System of Northern Pakistan. Peshawar Department of Civil Engineering, N-W.F.P. University of Engineering and Technology, Peshawar, Pakistan, 2009.
- Jemaa, (2007). Seismic design and analysis of reinforced concrete structures. Uk: university of sheffield.
- Journal of Earthquake Engineering, 12(S2):234–245, 2008 Copyright _ A.S. Elnashai & N.N. Ambraseys ISSN: 1363-2469 print / 1559-808X online DOI: 10.1080/13632460802014147

- Korkmaz, K.A., Demir, F. and Sivri, M. (2007) Earthquake Assessment of R/C Structures with Masonry Infill Walls. International Journal of Science & Technology, 2(2), pp. 155-164.
- Kyriakides N. (2007) Vulnerability of RC buildings and risk assessment for Cyprus, PhD Thesis, Department of Civil and Structural Engineering, University of Sheffield, UK.
- Lang, K. and Bachmann, H. (2004) on the seismic vulnerability of existing buildings: a case study of the city of basel. Earthquake Spectra, 20(1), pp. 43–66.
- Madan, A., Reinhorn, A.M., Mander, J.B. and Valles, R.E., 1997. "Modeling of Masonry Infill Panels for Structural Analysis". Journal of Structural Engineering, October, PP 1295 - 1302.
- Mekonnen Degefa (2005). Response of Masonry Infilled RC Frame under Horizontal Seismic Force. Master thesis, Addis Ababa University.
- Mohyeddin-Kermani1, A., Goldsworthy, H.M. and Gad, E. (n.d) A Review of the Seismic Behavior of RC Frames with Masonry Infill.
- Murty, C. V. R., Brzev S., Faison, H., Comartin, C.D. and Irfanoglu, A. (2006) The Seismic Performance of Reinforced Concrete Frame Buildings with Masonry Infill Walls. California: Earthquake Engineering Research Institute.
- P.G Asteris, M.ASCE (2011) Mathematical Macromodeling of Infilled Frames: State of the Art. Journal of Structural Engineering ASCE/December 2011.
- Palacios, S.M. (2004) State of The Art in Seismic Vulnerability.
- Paulay, T. and Priestley, M.J.N., 1992, Seismic Design of Reinforced Concrete and Masonry Buildings, John Wiley & Sons, New York.
- Paulay, T. and Priestly, M.J.N. (1992) Siesmic Design of reinforced concrete and masonary buildings. New York: Johns Wiley and Sons.
- Penelis, G. G. and Kappos, A. J., 1997. Earthquake Resistant Concrete Structures St. Edmundsbury Press Limited, Bury St. Edmunds, Suffolk.

- Pujol, S., Benavent-Climent, A., Rodriguez, M.E. and Smith-Pardo, J.P. (2008) Masonry infill walls: an effective alternative for seismic strengthening of low-rise reinforced concrete building structures. Beijing: The 14th World Conference on Earthquake Engineering.
- Rizwan, M. (2005) Performance evaluation of RC structure under earthquake loading. Lahore: Department Of Civil Engineering University Of Engineering And Technology
- Rossetto, t., & elnashai, a. (2003). Derivation of vulnerability functions for european-type RC structures based on observational data. Engineering structures, 1241-1263.
- Sattar, S. and Liel, A.B. Seismic performance of reinforced concrete frame structures with and without masonry infill walls. Boulder: Department of Civil, Environmental and Architectural Engineering, University of Colorado.
- Sezen, H. 2002. Seismic response and modeling of reinforced concrete building columns. Ph.D. thesis, Department of Civil and Environmental Engineering, University of California, Berkeley,Calif.
- Smyrou, E. (2006). Implementation and verification of a masonry panel model for non-linear dynamic analysis of infilled RC frame. Master thesis, European School for Advance Studies in Reduction of Seismic Risk, ROSE SCHOOL, Pavia, Italy.
- Stafford-Smith, B.S., 1966, “Behavior of square infilled frames,” ASCE (92)1: 381-403.
- Vulnerability Analysis for Gravity Load Designed RC Buildings in Naples – Italy Polese, M., Verderame, G.M., Mariniello, C., Iervolino, I. and Manfredi, G.
- WHE (2006) the Seismic Performance of Reinforced Concrete Frame Buildings with Masonry Infill Walls. Publication Number WHE-2006-03.
- Whitman, r., hong, s., & reed, j. (1973). Earthquake damage probablity matrices. Proceedings 5th world conference on earthquake engineering, (pp. 2531-2540). Rome.

Appendix A

Analytical Tool (PERFORM 3D)

PERFORM 3D (2006) was developed by Dr. Graham H. Powell, Professor of civil engineering in University of California at Berkeley (COMPUTERS AND STRUCTURES, INC. (CSI). PERFORM-3D is an advanced nonlinear tool which includes powerful capabilities of performance based design (COMPUTERS AND STRUCTURES, INC. (CSI), Website: http://www.csiberkeley.com).

For the nonlinear analysis of the structures various other computer programs are available such as ABAQUS, Open sees, ANSYS, SAP2000 and DRAIN 3D etc. Out of these programs, DRAIN 3D and PERFORM 3D are developed particularly for frame elements while others are general analytical softwares. In DRAIN 3D, model for inelastic shear is not available and take it as elasto-plastic. Further, DRAIN 3D is difficult to use as it lacks graphical user interface (GUI). PERFORM 3D is capable of modelling inelastic shear mechanism and material degradation. Therefore it is found suitable for this research work.

There are various type of elements in PERFORM 3D which are simple bar, column, beam, brace, shear wall, general wall, support spring and infill panel etc. As these elements are composed of components, hence, properties of the components are first defined to specify the properties of elements.

The several component types include:

- **Materials:** These include steel, concrete and shear materials for wall.
- **Cross Sections:** These include beam, column and wall sections of various types, such as column or beam standard steel section, column or beam RC section, column or beam steel type nonstandard section, column or beam inelastic fiber section, shear walls elastic and inelastic section, slab or shells inelastic sections.

- **Basic structural components:** These include bars, connection panel zones, plastic hinges, springs, seismic isolators and many others. Basic structural components then further categorized as elastic and in-elastic components. Elastic components cannot yield and dissipate energy while inelastic components can.
- **Compound components:** A compound component comprises of number of cross-sections, e.g., a beam compound component may consist of an elastic end zone component, a plastic hinge component and an elastic segment with a uniform cross section.

Concrete Material

Figure 1 shows the PERFORM hysteresis model for a concrete fiber in compression. The unloading stiffness is always equal to the initial elastic stiffness. The model controls the dissipated energy by changing the reloading stiffness. If the energy degradation factor is 1.0, reloading occurs as shown in Figure 1 (a). This is the maximum amount of energy dissipation. If the energy degradation factor is less than 1.0, reloading occurs as shown in Figure 1 (b). If the energy degradation factor is zero, the unloading and reloading lines are the same and there is no energy dissipation.

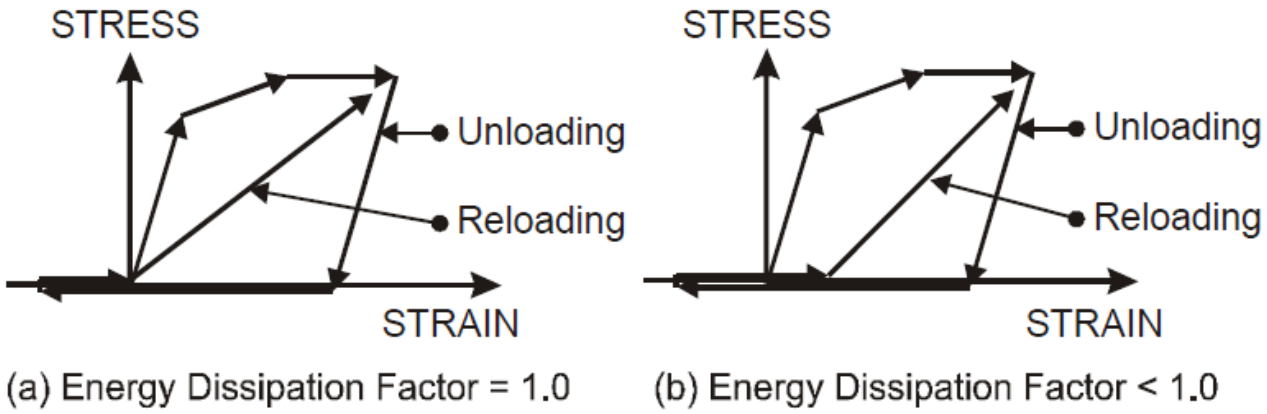

Figure1: Concrete Material in Compression

Concrete strength can be specified either finite or zero. If finite strength is specified, unloading and reloading are as shown in Figure 2, with no cyclic energy dissipation.

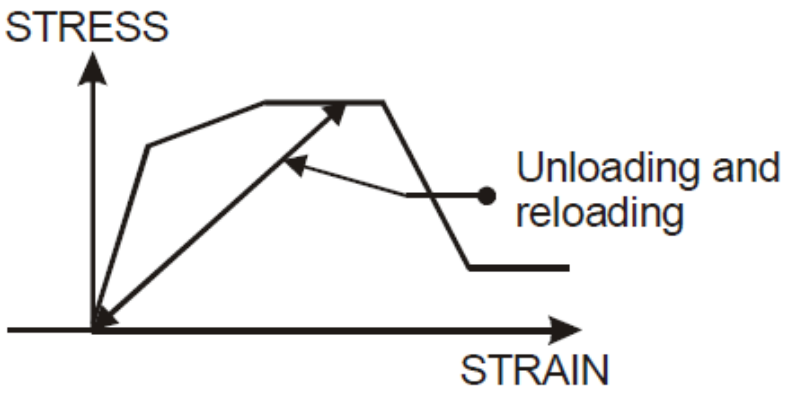

Figure2: Concrete Material in Tension

PERFORM assumes that the behavior in tension and compression are independent. Hence, crushing in compression does not affect subsequent tension behavior, and cracking in tension does not affect subsequent compression behavior.

Tension-Only Material (Steel)

The tension-only material is essentially the same as the concrete material, except that tension and compression are reversed.

Fiber Sections

A fiber cross section can have fibers of different types, usually steel and concrete. Fiber sections can be used for frame type elements and wall elements. There are two types of fiber cross section for beam and column elements, namely the “Beam Inelastic Fiber Section” and the “Column Inelastic Fiber Section”.

Beam sections use the fiber properties for axial force and in-plane bending only (usually vertical bending) and are elastic for out-of-plane bending (usually horizontal bending). Beam

sections account for P-M interaction for in-plane bending. Column sections use the fiber properties for bending about both axes, and account for P-M-M interaction.

The key aspect of a fiber segment is how it behaves when the fiber section becomes nonlinear, through yield of steel fibers and/or cracking and crushing of concrete fibers. PERFORM determines the behavior of a fiber cross section by monitoring the behavior of all of its fibers. However, this is done at only one section in each fiber segment, namely the section at the midpoint of the segment. For example, if a fiber section is made up entirely of steel fibers (i.e., if it models a steel cross section), the fiber segment yields only when the combination of axial force and bending moment at the midpoint of the segment is large enough to cause a fiber to yield. The bending moment, and hence the fiber stresses, will usually be a maximum at one end of the segment, but only the stresses at the segment midpoint are considered.

Shear Hinge

Beam and column sections are both assumed to be elastic for shear and torsion. If we want to consider inelastic shear behavior we must use shear hinge components. For inelastic shear we can use either a strain hinge or a displacement hinge, as explained in the following sections. A strain hinge is usually easier. It has the advantage that if we change the length of the shear link, the shear hinge properties are automatically updated. With a displacement hinge, if we change the shear link length we must recalculate the hinge properties.

Appendix B

CALCULATIONS FOR STRUCTURAL MODELLING

1. MASONRY INFILLS

Input Parameters

The recommended values for all these parameters are already discussed in section 2.2.3.4 and section 3.2.3.1.

Height of masonry = h_m = h_w = 123 in

Thickness of masonry = t = 9 in

Horizontal Length of masonry = L= 147 in

Diagonal Length of masonry = d_m= 192 in

Angle of diagonal strut = θ = 39.87 degrees

Elastic modulus of concrete = E_c = 3070544 Psi

Compressive strength of masonry = $f'm$ = 733.6 Psi (from experiments)

Elastic modulus of Masonry = E_m = 405130 Psi (using Equation 3-1)

Cracking stress of masonry = f_{tp} = 42.26 Psi

Geometrical Parameters

$$\frac{w}{d} = \frac{1}{4}$$

Total width of diagonal struts = w = 48 in

Area of diagonal strut = 216 in^2

Area of off-diagonal strut = 108 in^2

$$z = \frac{\pi}{2}.\lambda$$

$$\lambda = \sqrt[4]{\frac{4E_c\, I_c h_w}{E_m t sin(2\theta)}}$$

Separation between struts = *z/2* = 19.86 in

Mechanical Parameters

$$k_e = 2(E_m wt / L)(\cos\theta)^2$$

Initial stiffness of masonry infill panel = k_e = 386583 lbs/in

$$F_{\max} = 0.818\frac{L_{in}\, t\, f_{tp}}{C_I}(1+\sqrt{C_I{}^2+1}), \qquad C_I = 1.925\frac{L_{in}}{h'}$$

Maximum strength of infill = F_{max} = 69.82 kips

Ratio of cracking force to maximum strength = F_{cr}/ F_{max} = 0.55

Residual strength of masonry = F_r = 13.96 kips

Displacement at the maximum load along strut axis = δ_{cap} = 0.427 in

Displacement at the residual strength along strut axis = δ_c = 2.13 in

2. SHEAR ELEMENTS

Input Parameters

The recommended values for all these parameters are already discussed in section 2.3.1.5.

Concrete compressive strength = f'_c = 2900 Psi

Elastic modulus of concrete = E_c = 3070544 Psi

Steel Strength = f_y = 79915 Psi (Chaudat et al., 2005)

Axial load in 1st storey column = P = 21.46 Kips

Axial load in 1st storey column = P = 10.45 Kips

Aspect Ratio = a/d = 4

Ties Spacing in Columns = 7.87 in

Ties Spacing in beams = 11.8 in

F-D relationship for 1st storey columns

Length of column = L= 131 in

Effective depth = d = 9.053 in

Area of steel = A_s = 1.9 in^2

Moment capacity at yield = M_y = 341.6 Kip-in

$$V_y = 2M_y / L$$

Peak lateral strength = V_y = 5.216 Kips

$$P_o = 0.85 f'_c A_g (1 - \rho_l) + f_y A_{sl}$$

Axial load capacity = Po = 406 K

Axial load ratio = P/ P_o = 0.053

$$V_c = \frac{6\sqrt{f_c'}}{a/d}\sqrt{1+\frac{P}{6\sqrt{f_c'}A_g}}\,0.80A_g$$

Concrete capacity = V_c = 8.67 Kips

$$V_s = \frac{A_s f_{yw} d}{s}$$

Steel capacity = V_s = 8.065 Kips

$$V_n = V_c + V_s$$

Total Shear Capacity = V_n = 16.73 Kips

Residual Capacity = V_r = 11.71 Kips

$$\delta_{y,shear} = \left(\frac{3}{0.2+0.4P_r}\right)\frac{V_y L}{E_c A_g}$$

Yield displacement = δ_y = 0.0287 in

F-D relationship for 2nd storey columns

Length of column = L= 131 in

Effective depth = d = 9.053 in

Area of steel = A_s = 0.95 in^2

Moment capacity at yield = M_y = 203.83 Kip-in

Peak lateral strength = V_y = 5.216 Kips

Axial load capacity = P_o = 332 K

Axial load ratio = P/ P_o = 0.0314

Concrete capacity = V_c = 7.76 Kips

Steel capacity = V_s = 8.065 Kips

Total Shear Capacity = V_n = 15.82 Kips

Residual Capacity = V_r = 11.07Kips

Yield displacement = δ_y = 0.0248 in

F-D relationship for Beams

Length of column = L= 157 in

Effective depth = d = 14.56 in

Area of steel = A_s = 1.9 in^2

Moment capacity at yield = M_y = 757.6 Kip-in

Peak lateral strength = V_y = 9.616 Kips

Total Shear Capacity = V_n = 25.79 Kips

Residual Capacity = V_r = 18.05 Kips

Yield displacement = δ_y = 0.0381 in